

Horizons in a binary black hole merger I: Geometry and area increase

Daniel Pook-Kolb,^{1,2} Ofek Birnholtz,³ José Luis Jaramillo,⁴ Badri Krishnan,^{1,2} and Erik Schnetter^{5,6,7}

¹*Max-Planck-Institut für Gravitationsphysik (Albert Einstein Institute), Callinstr. 38, 30167 Hannover, Germany*

²*Leibniz Universität Hannover, 30167 Hannover, Germany*

³*Department of Physics, Bar-Ilan University, Ramat-Gan 5290002, Israel*

⁴*Institut de Mathématiques de Bourgogne (IMB), UMR 5584, CNRS, Université de Bourgogne Franche-Comté, F-21000 Dijon, France*

⁵*Perimeter Institute for Theoretical Physics, Waterloo, ON N2L 2Y5, Canada*

⁶*Physics & Astronomy Department, University of Waterloo, Waterloo, ON N2L 3G1, Canada*

⁷*Center for Computation & Technology, Louisiana State University, Baton Rouge, LA 70803, USA*

Recent advances in numerical relativity have revealed how marginally trapped surfaces behave when black holes merge. It is now known that interesting topological features emerge during the merger, and marginally trapped surfaces can have self-intersections. This paper presents the most detailed study yet of the physical and geometric aspects of this scenario. For the case of a head-on collision of non-spinning black holes, we study in detail the world tube formed by the evolution of marginally trapped surfaces. In the first of this two-part study, we focus on geometrical properties of the dynamical horizons, i.e. the world tube traced out by the time evolution of marginally outer trapped surfaces. We show that even the simple case of a head-on collision of non-spinning black holes contains a rich variety of geometric and topological properties and is generally more complex than considered previously in the literature. The dynamical horizons are shown to have mixed signature and are not future marginally trapped everywhere. We analyze the area increase of the marginal surfaces along a sequence which connects the two initially disjoint horizons with the final common horizon. While the area does increase overall along this sequence, it is not monotonic. We find short durations of anomalous area change which, given the connection of area with entropy, might have interesting physical consequences. We investigate the possible reasons for this effect and show that it is consistent with existing proofs of the area increase law.

I. INTRODUCTION

One of the remarkable predictions of general relativity is the existence of black holes, purely geometric objects in a curved spacetime which behave like compact physical objects in numerous physical situations, and can power the most energetic phenomena in our universe. The properties of spacetime near black holes are unlike anything observed in flat space, even for very large black holes where the curvature near the horizon is not necessarily large. One of these unusual phenomena is the existence of *closed trapped surfaces*. These are 2-dimensional closed surfaces which have the unusual property that even outgoing light rays emanating from the surface are convergent. Such surfaces cannot exist completely contained in flat spacetime regions. In fact, within classical general relativity, they can only exist in geodesically incomplete spacetimes, usually taken to indicate the presence of a singularity [1, 2]. *Marginally outer trapped surfaces* (MOTS) are limiting cases of trapped surfaces where the outgoing light rays have vanishing convergence. The outermost MOTS on a given constant time hypersurface, also known as an apparent horizon, can be shown locally to have the property of a one-way membrane, i.e. any material particle having fallen into it cannot cross it again. The outermost MOTS can also be shown to have non-decreasing area and furthermore these are found to satisfy the laws of black hole mechanics. Black hole spacetimes however contain a much wider variety of MOTSs which have interesting physical and geometric properties.

Numerous merger events where two black holes merge to form a larger remnant black hole have now been observed by gravitational wave detectors [3–8]. The number of detections will increase by orders of magnitude in the next years as the detectors become more sensitive and new generations of detectors are built. It is common to understand such mergers using event horizons. A well known example is [9], the “pair of pants picture”, which clearly shows the merger of two disjoint surfaces to yield a final horizon. How should one think of the merger process in terms of marginally trapped surfaces, and does this yield a picture analogous to the “pair of pants”?

The scenario of how two MOTSs merge has been recently established for the first time numerically, and is summarized in Fig. 1. This figure is obtained from a numerical solution of the full vacuum Einstein equations for the head-on collision of two unequal mass black holes. We start with simplest puncture initial data where the black holes have no spin or initial linear momentum, namely Brill-Lindquist initial data [10]. The initial data is prescribed on Euclidean space with two points (the “punctures”) removed. The data is time symmetric, i.e. the extrinsic curvature vanishes. The 3-metric h_{ab} is conformally flat: $h_{ab} = \Phi^4 \delta_{ab}$. The conformal factor at a point \mathbf{r} is

$$\Phi(\mathbf{r}) = 1 + \frac{m_1}{2r_1} + \frac{m_2}{2r_2}, \quad (1)$$

where r_1 and r_2 are the distances from \mathbf{r} to the two punctures, d the distance between the punctures, and m_1, m_2 are the bare masses associated with the punctures. The

ADM mass is seen to be $M_{\text{ADM}} = m_1 + m_2$. There turns out to be a rich variety of MOTSs even in this simple initial data; see [11] for a detailed study. We choose a particular configuration $m_1 = 0.5$ and $m_2 = 0.8$, and the initial coordinate separation between the two punctures is $d_0/M_{\text{ADM}} = 1$. For these parameters, there are initially only two disjoint MOTSs (representing the two black holes) surrounding the two punctures. Throughout, we state times in units of $\mathcal{M} := M_{\text{ADM}}/1.3$.

As we evolve this initial data using the Einstein equations, the result is shown in Fig. 1. This is the analog of the “pair of pants picture”. In this figure time goes vertically upwards and horizontal sections of the tubes yield sections of the MOTSs at a given time (the MOTSs are axially symmetric, and thus the full MOTS can be obtained by revolving these sections around their respective axes). The tubes in red and purple are the world tubes of the two individual MOTSs. These get closer to each other and eventually touch at a time labeled T_{touch} , and go through each other after T_{touch} . At a time $T_{\text{bifurcate}}$ which is somewhat earlier than T_{touch} , when the two horizons get sufficiently close to each other, a common MOTS is formed outside the individual ones. This common MOTS immediately bifurcates into an inner and outer branch shown respectively as a green mesh and in blue. The outer branch (in blue) becomes more symmetric and reaches an equilibrium state corresponding to a MOTS of a Schwarzschild black hole horizon. The inner branch on the other hand becomes increasingly distorted. Eventually it merges with the two individual MOTSs precisely at the time T_{touch} . Finally, the inner MOTS develops self-intersections immediately after T_{touch} . For reference, we find $T_{\text{touch}} \approx 5.53781 \mathcal{M}$ ($\approx 4.25985 M_{\text{ADM}}$) and $T_{\text{bifurcate}} \approx 1.37460 \mathcal{M}$ ($\approx 1.05738 M_{\text{ADM}}$).

It is useful to rephrase the above in terms of sections of the world tubes of Fig. 1. Before time $T_{\text{bifurcate}}$ the intersection of the world tubes with a Cauchy surface will consist of two disjoint spherical surfaces which we shall denote \mathcal{S}_1 and \mathcal{S}_2 . The 3-dimensional world tubes generated by them will be denoted \mathcal{H}_1 and \mathcal{H}_2 respectively. Between $T_{\text{bifurcate}}$ and T_{touch} , \mathcal{S}_1 and \mathcal{S}_2 continue to exist separately, but are now surrounded by a pair of marginally trapped surfaces which enclose both \mathcal{S}_1 and \mathcal{S}_2 . The inner of these is denoted $\mathcal{S}_{\text{inner}}$ and the outer one (the apparent horizon) by $\mathcal{S}_{\text{outer}}$. The world tubes generated by them are $\mathcal{H}_{\text{inner}}$ and $\mathcal{H}_{\text{outer}}$. At T_{touch} , \mathcal{S}_1 and \mathcal{S}_2 touch and at later times they go through each other while remaining spherical. Also at T_{touch} , $\mathcal{S}_{\text{inner}}$ coincides with $\mathcal{S}_1 \cup \mathcal{S}_2$, i.e. it forms a cusp. After T_{touch} , the cusps of $\mathcal{S}_{\text{inner}}$ develop into knots, i.e. self-intersections, which become larger with time. The eventual fate of \mathcal{S}_1 , \mathcal{S}_2 and $\mathcal{S}_{\text{inner}}$ is not yet known [12, 13]; these get closer to the punctures whence they become difficult to track numerically (though constraints on their possible dynamics follow from general results precluding the change of topology of Cauchy hypersurfaces during evolution [14, 15]). $\mathcal{S}_{\text{outer}}$ continues moving outwards becoming ever more symmetric as it reaches its final equilibrium fate.

These results were first reported in [16], and the numerical method is detailed in [11, 16]. In particular, the existence of self-intersecting MOTSs has been proven in detail with high accuracy (cf. also the recent [17]). A number of questions still remain to be answered about this scenario. These include understanding geometric properties of the world tubes such as the status of the area increase law, physical properties such as multipole moments, fluxes of energy across the horizons, and the stability properties. The goal of the present series of papers is to discuss these physical properties in detail for this same initial configuration. In this paper, the first of two parts, we shall discuss the geometric properties of the world tubes shown in Fig. 1. This includes the signature of the world tubes, the expansion of the ingoing null rays, and most importantly, the area increase law. The area of the final apparent horizon $\mathcal{S}_{\text{outer}}$ at late times is certainly larger than the sum of the areas of \mathcal{S}_1 and \mathcal{S}_2 at early times. Moreover, we can trace a sequence of surfaces which takes us from the initially disjoint surfaces \mathcal{S}_1 and \mathcal{S}_2 to the single final horizon $\mathcal{S}_{\text{outer}}$. However, the area does not increase monotonically along this sequence; there are in fact short durations of area *decrease* along this sequence. This fact needs an explanation, and might have important physical implications. In short, the geometrical quantities studied in this first paper show *how* the area increases. The second paper (henceforth paper II) addresses the question of *why* the area increases, i.e. the energy fluxes across the horizon.

The plan for the rest of the paper is the following. Sec. II sets up notation and briefly summarizes the basic notions and results that we shall use later. The behavior of MOTSs under time evolution, even for the simple case of a head-on collision, exhibits a rich variety of geometric and physical properties, and we will need the full machinery of quasi-local horizons to describe these features. For this reason we summarize different notions of quasi-local horizons, and we shall find it appropriate to modify existing terminology in some cases. Sec. III discusses a very basic geometric and physical aspect, namely the area of the MOTSs, and the status of the area increase law. This will involve issues such as the signature of the world tube and whether the MOTSs are future or past trapped. The classic area increase law for event horizons might lead us to believe that area should always increase to the future. The situation will be somewhat more complicated for us. While the area of the MOTS does increase overall, we find that there are small durations where this does not hold. Sec. IV studies in detail the expansion of the ingoing null normal. Future trapped surfaces have negative ingoing expansion everywhere, indicating the presence of a singularity to the future. We shall see that the dynamical horizons are not everywhere future trapped, and have portions with positive ingoing expansion. Sec. V studies the signature of the dynamical horizons and it shows that the horizons have both timelike and spacelike portions. Sec. VI revisits the area increase, and considers the correspondence of geometric fields on the horizon with prop-

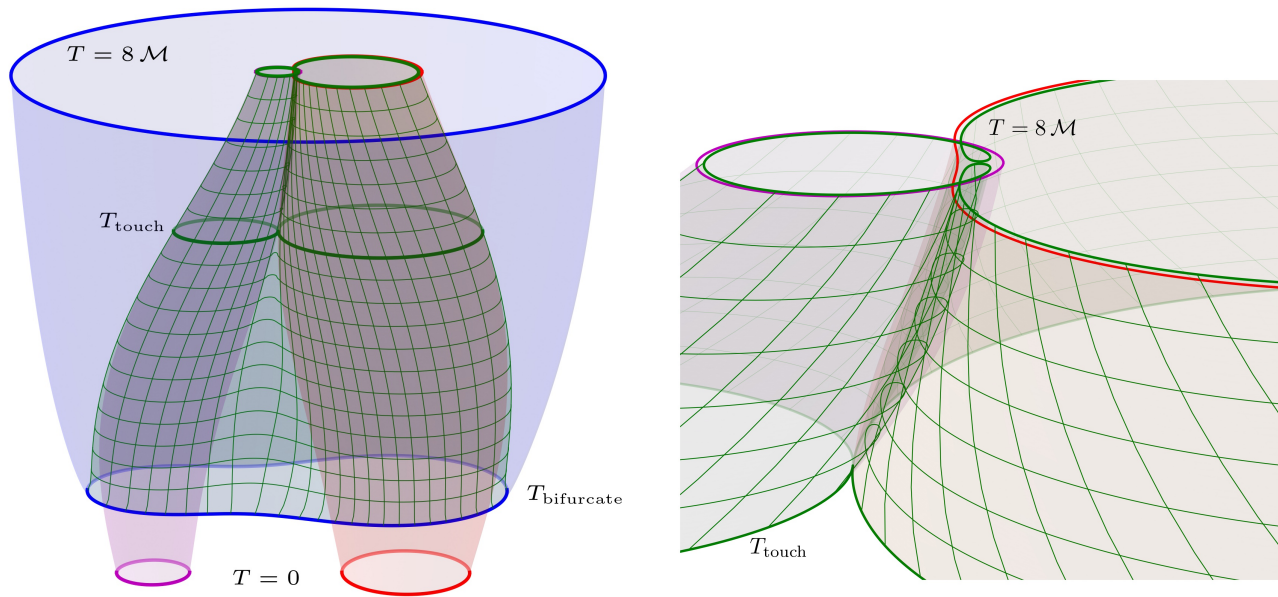


FIG. 1: The behavior of MOTSs in a binary black hole merger obtained from a numerical simulation of the full vacuum Einstein equations. The left panel shows an overview up to $T = 8\mathcal{M} > T_{\text{touch}}$ and the right panel a close-up of the end section of the two individual horizons (purple, red) and the inner common horizon (green) with the self-intersections visible. The blue contour describes the outer common horizon. See text for details.

erties of a 2-dimensional fluid, first suggested within the membrane paradigm. Sec. VII concludes by discussing open questions and possible directions for future work. Appendix A presents a detailed comparison of our results with the proof of area monotonicity on a dynamical horizon. Appendix B extends the membrane paradigm analogy to spinning black holes, and finally Appendix C speculates on a possible geometric interpretation of self-intersecting MOTSs.

II. BASIC NOTIONS

A. The optical scalars and marginally trapped surfaces

We collect here the basic notions and definitions related to quasi-local black hole horizons we shall need later. While we will try to be as self contained as possible, our goal in this section is not to provide a comprehensive overview of the subject, but rather to summarize the connections between the different notions with suitable references to the literature. Reviews with diverse viewpoints can be found in e.g. [18–25].

Spacetime is a 4-dimensional manifold \mathcal{M} with a Lorentzian metric g_{ab} with signature $(-, +, +, +)$. The derivative operator compatible with g_{ab} will be denoted ∇_a , and the Riemann tensor R_{abcd} is defined according to $(\nabla_a \nabla_b - \nabla_b \nabla_a)X_c = R_{abc}{}^d X_d$ for an arbitrary 1-form X_c . Let $\mathcal{S} \subset \mathcal{M}$ be a smooth, orientable, closed 2-dimensional spacelike surface. While it is possible to

consider higher genus surfaces, these are generically expected to be unstable [26] and we restrict ourselves to spherical topology in this paper. \mathcal{S} is naturally endowed with two null-normal fields denoted ℓ^a and n^a . These vector fields are required to be future-directed, null and orthogonal to \mathcal{S} . We are free to rescale them by positive-definite functions. This rescaling freedom can be reduced by fixing the inner-product $\ell \cdot n = -1$ which ties the rescalings of ℓ and n :

$$\ell \rightarrow f\ell, \quad n \rightarrow f^{-1}n, \quad f > 0. \quad (2)$$

Since \mathcal{S} is spacelike, the spacetime metric g_{ab} , when restricted to the tangent space of \mathcal{S} , yields a Riemannian metric

$$\tilde{q}_{ab} = g_{ab} + \ell_a n_b + n_a \ell_b. \quad (3)$$

We denote the volume 2-form on \mathcal{S} by $\tilde{\epsilon}_{ab}$, and the derivative operator on \mathcal{S} compatible with \tilde{q}_{ab} is denoted \mathcal{D} . Integrals over \mathcal{S} will be written with dA as the measure.

Of special importance for us will be the so called optical scalars, i.e. the expansion, shear, and twist of ℓ^a and n^a . The derivative $\nabla_a \ell_b$ projected on \mathcal{S} can be separated into a symmetric and anti-symmetric part, and the symmetric part can in turn be decomposed into a trace and trace-free part:

$$\tilde{q}_a^c \tilde{q}_b^d \nabla_c \ell_d = \frac{1}{2} \Theta_{(\ell)} \tilde{q}_{ab} + \sigma_{ab}^{(\ell)} + \omega_{ab}^{(\ell)}. \quad (4)$$

Here $\Theta_{(\ell)}$ is the *expansion* of ℓ^a , the symmetric tracefree tensor $\sigma_{ab}^{(\ell)}$ is the *shear*, and the anti-symmetric tensor

$\omega_{ab}^{(\ell)}$ is the *twist* of ℓ^a . The expansion, shear, twist of n^a are defined analogously:

$$\tilde{q}_a^c \tilde{q}_b^d \nabla_c n_d = \frac{1}{2} \Theta_{(n)} \tilde{q}_{ab} + \sigma_{ab}^{(n)} + \omega_{ab}^{(n)}. \quad (5)$$

The most important objects for us will be the two expansions, and $\sigma_{ab}^{(\ell)}$. In general, whenever we refer to shear or σ_{ab} , we shall mean $\sigma_{ab}^{(\ell)}$ unless indicated otherwise. The twist will vanish because, by construction, ℓ and n are orthogonal to a smooth surface \mathcal{S} .

It will often be useful to complete (ℓ, n) to a null-tetrad (ℓ, n, m, \bar{m}) where m^a is a complex null vector orthogonal to both ℓ and n . Thus m^a is tangent to \mathcal{S} and satisfies $m \cdot \bar{m} = 1$ (\bar{m} is the complex conjugate of m). Given the null-tetrad, the information contained in the symmetric-tracefree tensor σ_{ab} on \mathcal{S} can be reduced to a single complex field:

$$\sigma := \sigma_{ab} m^a m^b = m^a m^b \nabla_a \ell_b. \quad (6)$$

The choice of m can be changed by a phase: $m \rightarrow e^{i\psi} m$. Under this change, the shear transforms as $\sigma \rightarrow e^{2i\psi} \sigma$ which means that σ has spin weight +2. This implies that σ can be expanded into angular modes on \mathcal{S} using spin-weighted spherical harmonics of spin-weight +2. This will play a very important role in paper II.

The projections of $\nabla_a \ell_b$ and $\nabla_a n_b$ given in Eqs. (4) and (5) are the two extrinsic curvatures of \mathcal{S} embedded in spacetime \mathcal{M} . The other important quantity is the connection on the normal bundle of \mathcal{S} . Since \mathcal{S} has co-dimension 2, the connection on the normal bundle is given by a single 1-form ω_a defined as

$$\omega_a = -n_b \tilde{q}_a^c \nabla_c \ell^b. \quad (7)$$

This 1-form determines the angular momentum associated with the horizon; we will always deal with non-spinning black holes and will have $\omega_a = 0$ in this paper.

\mathcal{S} is said to be a *future-marginally-outer-trapped* surface if $\Theta_{(\ell)} = 0$ and $\Theta_{(n)} < 0$. Note that the expansions $\Theta_{(\ell)}$ and $\Theta_{(n)}$ are also rescaled under the transformation of Eq. (2), but these conditions remain unchanged since ℓ^a and n^a remain future directed. If instead $\Theta_{(n)} > 0$ (and still requiring $\Theta_{(\ell)} = 0$), then \mathcal{S} is said to be *past-marginally-outer-trapped*. We shall often just refer to *marginally trapped surfaces* with the understanding that we are referring to future-marginally-outer-trapped surfaces. Surfaces satisfying only $\Theta_{(\ell)} = 0$ (with no condition on $\Theta_{(n)}$) are the marginally outer trapped surfaces, or MOTS in short – these are the basic objects that we shall study in this paper. As we shall see, $\Theta_{(n)} < 0$ will not always be satisfied; it is therefore necessary to keep track of this condition in the various definitions and results.

A MOTS is a geometric concept in the full 4-dimensional spacetime independent of any spatial slices. In numerical simulations however, they are connected to Cauchy surfaces because in order to locate them, we only

require the Cauchy data, i.e. the 3-metric and extrinsic curvature. For a closed 2-surface \mathcal{S} in Σ , let R^a be the spacelike outward pointing normal to \mathcal{S} , and T^a the unit-timelike normal to Σ . A convenient choice for the null normals is

$$\ell^a = \frac{1}{\sqrt{2}} (T^a + R^a), \quad n^a = \frac{1}{\sqrt{2}} (T^a - R^a). \quad (8)$$

The expansion condition $\Theta_{(\ell)} = 0$ can be written in terms of the extrinsic curvature K_{ab} of $\Sigma \subset \mathcal{M}$:

$$D_a R^a + K_{ab} R^a R^b - K = 0 \quad (9)$$

where D_a is the derivative operator on Σ . Taking \mathcal{S} to be the level set of a suitable function h , this equation can, in turn, be expressed as a second order non-linear differential equation for h . Our choice for h is based on choosing a reference surface sufficiently close to \mathcal{S} . Details on how the reference surface is chosen, the associated co-ordinate system, and the numerical method for solving the above equation can be found in [11, 27] and our implementation is available at [28]. This is an extension of the widely used method developed in [29–34]. Our numerical calculations use the *Einstein Toolkit* [35, 36]. We use *TwoPunctures* [37, 38] to set up initial conditions and an axisymmetric version of *McLachlan* [39] to solve the Einstein equations, which uses *Kranc* [40, 41] to generate efficient C++ code. For the results in the current series of papers, we performed simulations with three spatial resolutions $1/\Delta x = 960, 480, 60$, running, respectively, until $T_{\max} = 7\mathcal{M}, 20\mathcal{M}, 50\mathcal{M}$. Further details of the simulation specific to our problem are detailed in [27].

We now collect basic definitions and results pertaining to quasi-local horizons that we shall use while presenting our results. The goal here is not a detailed review of the subject, but mainly to orient the reader and to set up notation and terminology.

B. The MOTS stability operator

Starting with a MOTS on a Cauchy surface, it is natural to ask how it behaves under time evolution. It is not *a priori* obvious that a MOTS should evolve smoothly. It is now known that the behavior of a MOTS under time evolution is controlled by a second order non-self-adjoint elliptic operator L_Σ known as the stability operator [11, 42–44]. L_Σ is constructed from variations of \mathcal{S} [26]. Given a surface \mathcal{S} , let \mathcal{S}_λ be a family of surfaces parameterized by a real variable λ ; the surfaces \mathcal{S}_λ depend smoothly on λ . We take $\mathcal{S}_{\lambda=0}$ to coincide with \mathcal{S} , and λ can take values in an interval $(-\epsilon, \epsilon)$. The variation \mathcal{S}_λ is assumed to be smooth which implies that if we pick a point p on \mathcal{S} , the variation produces a smooth curve passing through p , and the tangent vector to these curves at $\lambda = 0$ defines a vector field X on \mathcal{S} . With this structure, one can naturally define the variation of geometric quantities on \mathcal{S} [45, 46]. Of particular importance is the

variation of $\Theta_{(\ell)}$ denoted $\delta_X \Theta_{(\ell)}$. On each \mathcal{S}_λ construct the null normals $\ell^{(\lambda)}$ and $n^{(\lambda)}$ as for \mathcal{S} itself. This defines the expansion $\Theta_{(\ell)}^{(\lambda)}$ for all λ , and allows us to differentiate it:

$$\delta_X \Theta_{(\ell)} := \left(\frac{d\Theta_{(\ell)}^{(\lambda)}}{d\lambda} \right)_{\lambda=0}. \quad (10)$$

This variation should not be confused with usual derivatives of $\Theta_{(\ell)}$. In particular, while $\delta_{cX} \Theta_{(\ell)} = c\delta_X \Theta_{(\ell)}$ for constants c , it turns out that $\delta_{\psi X} \Theta_{(\ell)} \neq \psi\delta_X \Theta_{(\ell)}$ if ψ is a non-constant function. If X is tangent to \mathcal{S} and $\Theta_{(\ell)} = 0$ on \mathcal{S} , then it is obvious that $\delta_X \Theta_{(\ell)} = 0$. Thus, we only need to consider variation fields X normal to \mathcal{S} . One could consider X to be proportional to ℓ or n , but in the context of a Cauchy evolution, it is natural to take X along the normal R^a , $X^a = \psi R^a$. Thus, we define the stability operator associated with $\Sigma \supset \mathcal{S}$ as

$$L_\Sigma [\psi] := \sqrt{2} \delta_{\psi R} \Theta_{(\ell)}, \quad (11)$$

where a global constant positive factor can be arbitrarily chosen, and $\sqrt{2}$ is chosen to simplify later expressions. An explicit calculation shows that L_Σ is a second order elliptic operator but it is not necessarily self-adjoint. In vacuum spacetimes, the expression for L_Σ is the following:

$$L_\Sigma [\psi] = -\Delta_{\mathcal{S}} \psi + 2\omega^a \mathcal{D}_a \psi + \left(\frac{1}{2} \mathcal{R} + \mathcal{D}_a \omega^a - \omega_a \omega^a - \sigma_{ab} \sigma^{ab} \right) \psi. \quad (12)$$

Here $\Delta_{\mathcal{S}}$ is the Laplacian on \mathcal{S} and \mathcal{D}_a is the derivative operator on \mathcal{S} . In the present case, we shall deal with the head-on collision of non-spinning black holes so that $\omega_a = 0$, whence L_Σ will be self-adjoint and will have real eigenvalues.

In the dynamical evolution setting, the importance of L_Σ lies in the following result [11, 42–44]:

- *A MOTS evolves smoothly as long as L_Σ is invertible, i.e. as long as none of its eigenvalues vanish.*

In simple cases when the smallest eigenvalue Λ_0 is strictly positive, then L_Σ is obviously invertible and the MOTS evolves smoothly. In a binary black hole merger, this is what happens for the outermost MOTS and the two individual MOTSs. However, as shown in [11, 16, 27], the inner common MOTS is more complicated. It is born at $T_{\text{bifurcate}}$ with $\Lambda_0 = 0$ which immediately becomes negative. None of the other eigenvalues cross 0 and the MOTS continues to evolve smoothly. It is clear from this that the complete spectrum of L_Σ , and not just its principal eigenvalue, is potentially of interest. This is especially true for spinning black holes when the eigenvalues can be complex, thus leading to the full MOTS-spectral problem formulated in [47] and initiated in [48, 49]. We shall explore the spectrum of L_Σ in paper II.

C. Marginally trapped tubes and dynamical horizons

With the time evolution understood, we consider the three-dimensional world tube traced out by a MOTS. This world tube is known as a *marginally outer trapped tube*. More formally (following [43]):

Definition 1 (Marginally Outer Trapped Tube). *A smooth 3-dimensional surface \mathcal{H} in a spacetime is said to be a marginally outer trapped tube (MOTT) if*

- *it has topology $S^2 \times \mathbb{R}$, i.e. it admits a foliation by 2-spheres,*
- *each leaf of the foliation is a MOTS.*

Note that \mathcal{H} is allowed to have arbitrary signature and no restrictions are placed on the ingoing expansion $\Theta_{(n)}$ for any of the MOTSs which constitute \mathcal{H} . As we have seen, the results involving the stability operator mentioned above do not assume any condition on $\Theta_{(n)}$, and hold for any MOTT. The classic examples of MOTTs in spherical symmetry are the well known Vaidya [50] and Oppenheimer-Snyder [51] solutions. Further examples in spherical symmetry can be found in e.g. [52–54]. These examples already show the wide variety of cases that can appear even in spherical symmetry. See [55] for a construction of the spacetime locally near such a horizon. See e.g. [12, 34, 56, 57] for previous examples of numerical studies concerning dynamical horizons in various physical situations. The present paper shall provide the most detailed numerical study yet of these horizons in a black hole merger.

Imposing additionally $\Theta_{(n)} < 0$ leads to the definition of a marginally trapped tube (following [58]):

Definition 2 (Marginally Trapped Tube). *A MOTT is said to be a marginally trapped tube (MTT) if it satisfies in addition $\Theta_{(n)} < 0$ everywhere.*

As we shall discuss below in Sec. III, the condition $\Theta_{(n)} < 0$ is employed in different proofs of the area increase law. The proof of the area increase law [59–61] holds for an MTT of arbitrary signature, though with additional technical assumptions we shall discuss later (MTTs are referred to as holographic screens in this work).

Additional restrictions can be placed on a MOTT depending on the physical situation one is interested in. When the marginally trapped tube is in equilibrium, i.e. there is no energy flux across \mathcal{H} , we need the notion of a non-expanding horizon [62]:

Definition 3 (Non-expanding horizon). *A smooth 3-dimensional surface Δ in a spacetime is said to be a non-expanding-horizon if*

- Δ *has topology $S^2 \times \mathbb{R}$*
- Δ *is null*

- Any null normal to Δ , denoted ℓ^a , has vanishing expansion ($\Theta_{(\ell)} = 0$).
- The Einstein field equations hold at Δ and, if T_{ab} is the stress energy tensor, $-T_b^a \ell^b$ is future directed and causal when ℓ^a is future directed.

From the properties of a null surface, it can be shown that every complete cross-section of Δ is a MOTS. Thus, a non-expanding horizon is, in essence, a MOTT with null signature. The last condition is an energy condition and is implied by, for example, the dominant energy condition. It can also be shown that each cross-section of Δ has the same area; the black hole here is in equilibrium in an otherwise dynamical spacetime. Not all geometric fields on a non-expanding horizon are time independent. Further physical restrictions requiring the derivative operator to be time independent lead to the notion of an isolated horizon [63–65]. It is interesting to note that a version of the stability operator also appears in going from non-expanding to isolated horizons [65], and again, the invertibility of the stability operator turns out to be the relevant condition.

Local constructions of spacetime neighborhoods near non-expanding horizons is given in [55, 63, 66–71]. All stationary black holes and Killing horizons, including of course the Schwarzschild and Kerr black holes, are non-expanding horizons. A detailed study of the Kerr-Newman black hole viewed as a non-expanding horizon can be found in [72]. Apart from these, there are also the so-called distorted black holes representing stationary black holes in the presence of external fields [73] (see also [74] for exact solutions representing charged distorted black holes). Distorted black holes can potentially have positive $\Theta_{(n)}$ [75].

Moving now to the general dynamical case, we will work with a general MOTT. As we shall see, a MOTT can be spacelike or timelike, or even have sections of mixed signature. In addition it can have positive or negative $\Theta_{(n)}$. In principle we could add qualifiers in front of MOTT and refer to, for example, spacelike or timelike MOTTs. However, to minimize the number of acronyms and to perhaps make it easier to remember:

Definition 4 (Dynamical Horizons). *We shall refer to a generic MOTT as a dynamical horizon. Additional qualifiers will be added as appropriate. Thus we can have spacelike or timelike dynamical horizons depending on the signature, and future or past depending on whether $\Theta_{(n)} < 0$ or > 0 respectively.*

The reader might be aware that previously, dynamical horizons referred to spacelike MTTs [76, 77] (this is closely related to but not the same as a future outer trapping horizon [78–81]). However, already in [77] (Appendix B), timelike cases were considered and referred to as timelike dynamical horizons. Dynamical horizons were always meant to refer to a general MOTT and the spacelike case was initially thought to be the most relevant case. We shall therefore use different terminology in

this paper. A general MOTT will be called a dynamical horizon and qualifiers will be added as appropriate.

We conclude this section by a short discussion of the area increase and fluxes across dynamical horizons. Consider a portion $\Delta\mathcal{H}$ between two MOTSs with initial area A_i and final area A_f . As shown in [45, 76, 82], the area change $A_f - A_i$ can be written as an integral over $\Delta\mathcal{H}$, with the integrand being local fields on $\Delta\mathcal{H}$. The integrand can be viewed as a flux, whence the area is seen to change due to the flux of radiation across the horizon. We shall discuss the fluxes in great detail in paper II, but here we just mention two points: i) the dominant contribution is due to the shear $\sigma_{ab}^{(\ell)}$, which was recently seen to be closely correlated with the outgoing flux measured at infinity [83]. Thus, the fluxes provide a critical link between horizon dynamics and observations of gravitational waves. ii) the fluxes are manifestly positive definite for spacelike dynamical horizons, but not so for timelike cases [77].

Besides these flux laws, there is an alternate formulation of the area change. The starting point is the membrane paradigm for black hole event horizons [84–87]. By applying the Einstein equations to an event horizon, Damour showed a close analogy between evolution equations on the horizon and the Navier-Stokes equation for a 2-dimensional fluid [84, 85]. In this way, it is possible to relate fields on the event horizon and physical properties of a corresponding 2-dimensional fluid such as energy density, pressure, bulk and shear viscosity. An interesting feature of this correspondence is that one obtains a negative bulk viscosity for the fluid, suggesting an instability. As shown in [88–90], this correspondence also holds for dynamical horizons and one can similarly obtain counterparts to the various physical quantities listed above. In particular, the bulk viscosity now turns out to be positive as expected. We shall explore certain aspects of this analogy later in Sec. VI.

III. THE AREA INCREASE LAW

The laws of black hole thermodynamics can be satisfactorily formulated using quasi-local horizons [62, 64, 76, 77, 91–93]. For example, formulations of the first law of black hole mechanics based on event horizons [94, 95] use a mixture of quantities defined at the horizon (such as the area) and infinity (such as the ADM mass, and also surface gravity which uses the timelike Killing vector normalized at infinity). The quasi-local formulation of the first law satisfactorily addresses this problem, and coherently uses quantities defined only at the horizon. Here we shall not review all aspects of black hole thermodynamics, and instead focus on one aspect, namely the area increase law.

The areas of the various horizons for our particular configuration are straightforward to calculate and have been presented previously [16, 27]. Here we present the same data first in terms of the radii of the black holes;

see Fig. 2. For a spherical surface with area A , one can define a radius R according to $\sqrt{A/4\pi}$, known as the area-radius. This is straightforward to define for $\mathcal{S}_{\text{inner}}$ and $\mathcal{S}_{\text{outer}}$, and their radii will be denoted R_{inner} and R_{outer} respectively. For the two individual horizons \mathcal{S}_1 and \mathcal{S}_2 , we can similarly define an effective area radius R_{1+2} as $\sqrt{(A_1 + A_2)/4\pi}$. Fig. 2 plots these radii as functions of time. To connect the two initial horizons to the final one, one can follow the curves along the segment *I*, then follow segment *II* backwards in time, and then segment *III* which takes us to the final remnant black hole. While the overall area change is of course positive, the area does not change monotonically along *I* + *II* + *III*. There is a small duration of anomalous area increase on segment *II* just prior to T_{touch} . The second panel shows a close-up near T_{touch} and the anomalous area increase of $\mathcal{S}_{\text{inner}}$. For reference, the local minimum of the area occurs at $T_{\text{min}} = 5.50594 \mathcal{M}$.

Fig. 3 shows the irreducible masses $M_{\text{irr}} = \sqrt{A/16\pi}$ of the various horizons. For the two individual horizons \mathcal{S}_1 and \mathcal{S}_2 , we show them separately and also the sum

$$M_{\text{irr}}^{(1)} + M_{\text{irr}}^{(2)} = \sqrt{A_1/16\pi} + \sqrt{A_2/16\pi}. \quad (13)$$

This measure takes into account the interaction energy between the two black holes, which in fact is quite significant given that the separation between the black holes is small. Thus unlike Fig. 2, in Fig. 3, the curve for $M_{\text{irr}}^{(1)} + M_{\text{irr}}^{(2)}$ lies above the curves for the outer horizons. For the apparent horizon, the value of $M_{\text{irr}}^{\text{outer}}$ at late times is a good approximation to the Bondi mass, i.e. the mass left in the spacetime after all the gravitational radiation has left the system. Since this is a very short simulation, the amount of radiation is small and the difference between this estimate of the Bondi mass and the ADM mass is smaller than 0.1%.

In the next sections we will go deeper into the various ingredients which determine the area change. Let us therefore conclude this section by outlining why the expansion $\Theta_{(n)}$, and the signature of the dynamical horizons, are the main ingredients we should be looking at. There are some simplified cases when the area increase law can be easily proved, namely for purely future-spacelike and purely future-timelike dynamical horizons, i.e. we assume everywhere $\Theta_{(n)} < 0$ and fix the signature. Let us start with the spacelike case, and let \mathcal{H} be the dynamical horizon. The null normal choices of Eq. (8) are tied to a Cauchy surface intersecting the dynamical horizon. We need instead null-normals entirely determined by \mathcal{H} . Since \mathcal{H} is spacelike, it has a unit-timelike normal $\hat{\tau}^a$. The foliation on \mathcal{H} determines a unit-spacelike vector field \hat{r}^a , which we take to be outward pointing. Then, analogous to Eq. (8), a suitable choice of null normals is

$$\hat{\ell}^a = \frac{\hat{\tau}^a + \hat{r}^a}{\sqrt{2}}, \quad \hat{n}^a = \frac{\hat{\tau}^a - \hat{r}^a}{\sqrt{2}}. \quad (14)$$

Then, with $\Theta_{(\hat{\ell})} = 0$, we easily get

$$D_a \hat{r}^a = -\frac{\Theta_{(\hat{n})}}{\sqrt{2}} > 0, \quad (15)$$

where D_a is the derivative operator on \mathcal{H} . This shows that the area of the cross-sections of \mathcal{H} increases along \hat{r}^a . Similarly, for a timelike dynamical horizon, the roles of \hat{r}^a and $\hat{\tau}^a$ are interchanged and it is now $\hat{\tau}^a$ which is tangent to \mathcal{H} . We get for the divergence of $\hat{\tau}^a$:

$$D_a \hat{\tau}^a = +\frac{\Theta_{(\hat{n})}}{\sqrt{2}} < 0, \quad (16)$$

whence the area decreases along $\hat{\tau}^a$. The reader should bear in mind that the null normals \hat{n}^a and n^a are related by a scaling as in Eq. (2). Thus the expansions of \hat{n}^a and n^a are also related by a scaling, but the sign of the expansion remains unchanged.

These simple calculations illustrate the importance of the sign of $\Theta_{(n)}$ and the signature. The proof of the area increase law by Bousso & Engelhardt [59, 60] which we will discuss below, does not make any assumption on the signature but does assume $\Theta_{(n)} < 0$. With this assumption, and additional technical requirements which will be important, it can be shown that the area must be monotonic on a future dynamical horizon. Now, viewing $\mathcal{H}_{\text{inner}}$ and $\mathcal{H}_{\text{outer}}$ as a single dynamical horizon (i.e. consider the union of the segments *III*, *II*, and *II'* shown in Fig. 2), the area is in fact monotonic *except for the anomalous area increase starting from T_{min}* . We need to explain which of the conditions assumed in the proof are violated. Some obvious questions for us are thus: Do the various dynamical horizons behave as one might have naively expected? For example, is the outer common horizon everywhere spacelike and does it have $\Theta_{(n)} < 0$? Similarly, is the inner horizon always timelike? What happens during the anomalous area increase shown in the second panel of Fig. 2? We shall now proceed to address these questions.

In the next sections we shall examine the signature and the behavior of $\Theta_{(n)}$ for all the horizons. Keep in mind the different role played by these two aspects: $\Theta_{(n)}$ is part of the extrinsic curvature of a MOTS, i.e. it is determined by how \mathcal{S} is embedded in a spacetime manifold. The signature of the dynamical horizons \mathcal{H} , on the other hand, necessarily involves MOTSs at different time steps; we need to obtain at least a small portion of \mathcal{H} in order to evaluate its signature. Thus, we first investigate $\Theta_{(n)}$ followed by the signature.

IV. THE EXPANSION OF THE INGOING NULL RAYS

As we have seen, the expansion of the inward pointing null rays, $\Theta_{(n)}$, is of great importance for the area increase law. The average $\overline{\Theta_{(n)}}$ over a closed 2-surface \mathcal{S} with area $A_{\mathcal{S}}$ and area 2-form $\tilde{\epsilon}$ is

$$\overline{\Theta_{(n)}} = \frac{1}{A_{\mathcal{S}}} \oint_{\mathcal{S}} \Theta_{(n)} \tilde{\epsilon}. \quad (17)$$

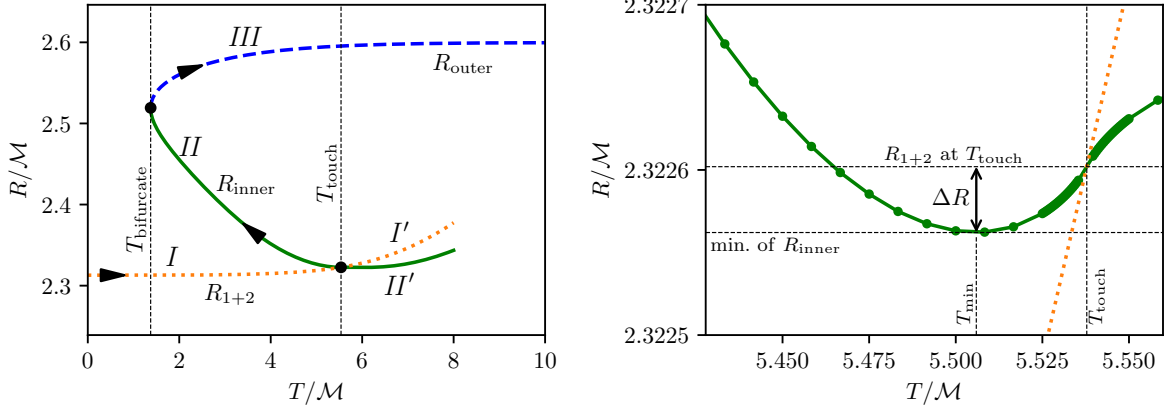


FIG. 2: The first panel shows the radii of the various horizons as functions of time. The orange dotted line is an “effective” area-radius for the two individual horizons, the blue curve is the radius of the apparent horizon, while the solid green curve is the radius of the inner common MOTS. It is possible to connect the initial radii with the final one by following the segment $I + II + III$ (the segment II is followed backwards in time). The second panel shows a close-up near T_{touch} where an anomalous increase in the area of the inner common horizon is observed.

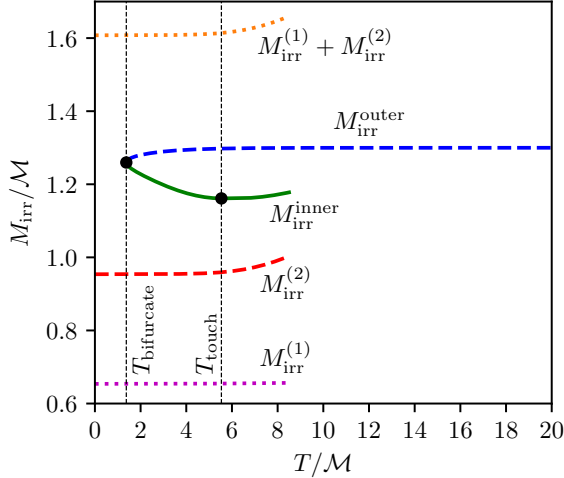


FIG. 3: Irreducible masses of the various horizons as functions of time.

The average of $\Theta_{(n)}$ is shown in Fig. 4 for all four horizons as functions of time. The initial data is time symmetric, which implies that $\Theta_{(n)} = 0$ for $\mathcal{S}_{1,2}$ initially. The average becomes negative and remains negative at all times. The common horizons are born with negative $\overline{\Theta}_{(n)}$ and they remain negative at all times.

The behavior of $\Theta_{(n)}$ beyond the averages is more interesting. The individual horizons however remain boring: $\Theta_{(n)} \leq 0$ for the individual horizons at all times. Since the initial data is time symmetric, the individual black holes initially have $\Theta_{(n)} = 0$ but it is strictly negative thereafter. The individual horizons are therefore conventional future-dynamical horizons. The outer dynamical horizon generated by the apparent horizons are somewhat more interesting: they do not always have $\Theta_{(n)} < 0$

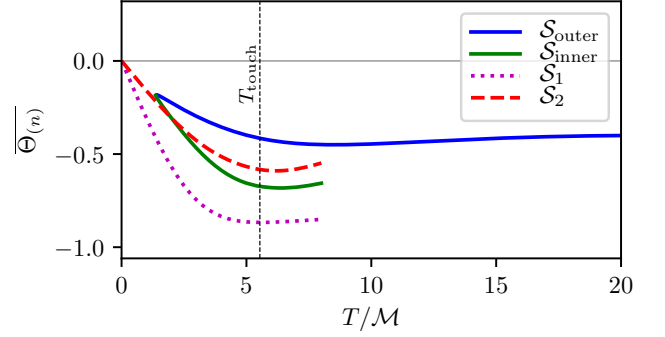


FIG. 4: The average ingoing expansion

as one might have expected. Upon formation, there is a small region with $\Theta_{(n)} > 0$ around the “waist” defined as follows. Each MOTS is axisymmetric, and thus has an axial symmetry vector φ^a . This vanishes at two points which defines the two poles. We can calculate the proper length of each orbit of φ^a . The proper length vanishes at the poles and, for a regular round sphere, it is maximum at the equator. However, for some of the MOTSs in our problem, we find that the proper circumference has a local minimum around the equator. This is most obvious for $\mathcal{H}_{\text{inner}}$ near T_{touch} where it looks like a figure eight (see second panel of Fig. 6), but it is also true for the apparent horizon just when it is born at $T_{\text{bifurcate}}$.

For $\mathcal{H}_{\text{outer}}$, this portion soon disappears and we have the conventional $\Theta_{(n)} < 0$ at all points on the apparent horizons after this. See Fig. 5. A similar feature was also seen in [57]. Evidently, the small portion with the “wrong” sign of $\Theta_{(n)}$ does not affect the area increase law for $\mathcal{H}_{\text{outer}}$; the relevant portion of the horizon is too small to have an overall effect and the apparent horizon

area is monotonically increasing.

As might be expected, the inner horizon $\mathcal{S}_{\text{inner}}$ is yet more interesting. As shown in Fig. 6, $\mathcal{S}_{\text{inner}}$ never truly becomes future marginally trapped, i.e. it always has a portion (around its “waist”) with positive $\Theta_{(n)}$. This shrinks with time and eventually vanishes momentarily at T_{touch} , but reappears immediately afterwards. Thus we see that $\mathcal{H}_{\text{inner}}$ is never truly future marginally trapped. However, just after $T_{\text{bifurcate}}$, $\mathcal{S}_{\text{inner}}$ is decreasing in area (as it should) despite this effect.

We see then that *dynamical horizons generally do not have $\Theta_{(n)} < 0$ everywhere* – this is the takeaway message from this section. This condition has been widely used in previous literature on quasi-local horizons to prove the area increase law. In particular, it is used in the proof of the area increase law for future dynamical horizons of arbitrary signature [59, 60]. Thus, these proofs are not directly applicable for $\mathcal{H}_{\text{inner}}$ and there is, strictly speaking, no contradiction. However, there is a more subtle reason why the proof of [59, 60] does not apply to $\mathcal{H}_{\text{inner}}$, and we shall return to this point shortly.

V. THE SIGNATURE OF THE DYNAMICAL HORIZONS

Given a MOTS and a dynamical horizon \mathcal{H} obtained by evolving it, the signature of \mathcal{H} can be computed in a straightforward way. For any point p on the world tube, we can construct three linearly independent vectors tangent to \mathcal{H} , say \mathbf{e}_A ($A = 1, 2, 3$) and find their inner-products $q_{AB} := \mathbf{e}_A \cdot \mathbf{e}_B$. The eigenvalues of q_{AB} then yield the signature; if it has a negative eigenvalue it is timelike, and it is spacelike if all eigenvalues are positive. If the matrix is degenerate then \mathcal{H} is a null surface.

Alternatively, we can consider properties of a “time evolution” vector on the dynamical horizon. Consider a dynamical horizon \mathcal{H} of arbitrary signature and arbitrary $\Theta_{(n)}$. Let V^a be a vector field on \mathcal{H} such that it is orthogonal to the leaves of the MOTSs which constitute \mathcal{H} , and it maps one foliation to the next. Thus, if on a dynamical horizon the MOTSs are labeled by a parameter λ , then we can choose λ such that $V^a \partial_a \lambda = 1$. Each MOTS \mathcal{S} is taken to lie on a given Cauchy surface and thus equipped with null normals (ℓ^a, n^a) according to Eq. (8). Since V^a is orthogonal to \mathcal{S} , there must exist functions b and c on \mathcal{S} such that

$$V^a = b\ell^a + cn^a. \quad (18)$$

Since $\ell \cdot n = -1$, we have $V \cdot V = -2bc$. Thus, the signature of \mathcal{H} is controlled by the sign of bc ; \mathcal{H} is spacelike if b and c have different signs, and timelike if they have the same signs. Readers more familiar with T^a and R^a might find the following expression for V^a more illuminating:

$$\sqrt{2}V^a = (b+c)T^a + (b-c)R^a. \quad (19)$$

We identify the 4 cases shown in Fig. 7 depending on the signs of b and c . If b and c are both positive, then

intuitively, the term along T^a dominates and is positive and thus V^a is timelike. Similarly, when b and c have opposite signs, the term along R^a dominates. When $b > c$, i.e. when $b > 0$ and $c < 0$, V^a points outwards (i.e. along R^a by definition), and in the opposite case when $b < c$ then it points inwards. We note that in our simulations, by construction the MOTS is found on Cauchy surfaces referring to a given time, and we essentially construct V^a by connecting a MOTS at a given time with another MOTS at a later time. This means that when it is timelike, V^a can never be past directed and thus case IV cannot occur in our simulations.

The null case corresponds to either of b or c vanishing, and it is usually assumed that this does not occur on open sets (this is borne out in our numerical results). The null portions arise when \mathcal{H} transitions between any two of the four cases listed above. Furthermore, only one of the signs can change in a transition; the vanishing of both b and c means that V^a vanishes which cannot happen as long as the foliation of the MOTT is regular. If $\tilde{\epsilon}$ is the area 2-form on \mathcal{S} , and when \mathcal{S} is a MOTS so that $\Theta_{(\ell)} = 0$, then

$$\mathcal{L}_V \tilde{\epsilon} = c\Theta_{(n)} \tilde{\epsilon}. \quad (20)$$

Locally, the area increase is determined by the product $c\Theta_{(n)}$. Thus, c plays a double role: the product bc determines the signature while the product $c\Theta_{(n)}$ determines the change in area. V^a is strictly null only on a set of measure zero. As discussed earlier, the null case is nevertheless very important for conceptual reasons. All of the well known stationary Kerr and Schwarzschild horizons are null. Moreover, $\mathcal{H}_{\text{outer}}$ has b large and positive, and c small but negative in the limit of late times as it reaches equilibrium, so that $V \cdot V = -2bc \gtrsim 0$. The same holds for \mathcal{H}_1 and \mathcal{H}_2 at early times.

With this understanding, we can now present our results regarding the signature. \mathcal{H}_1 , \mathcal{H}_2 and $\mathcal{H}_{\text{outer}}$ always turn out to be spacelike; this is consistent with them being stable in the sense of the principal eigenvalue of the stability operator being positive [43] (this will be discussed further in paper II). Only $\mathcal{H}_{\text{inner}}$ shows interesting behavior in this regard. The signature of this world tube is shown in Figs. 8. As discussed earlier, this horizon develops cusps and self intersections. From Fig. 8 we see clearly that $\mathcal{H}_{\text{inner}}$ is mostly timelike, but there are interesting and non-negligible portions which are spacelike. When it is initially formed at $T_{\text{bifurcate}}$, it is completely spacelike; it must of course agree there with $\mathcal{H}_{\text{outer}}$ which is always spacelike. However, it remains fully spacelike for only a few time-steps after which most portions become timelike; the region around the “waist” remains spacelike for the longest. After this, $\mathcal{H}_{\text{inner}}$ remains entirely timelike until just before T_{touch} when the portion around the *larger* black hole develops spacelike portions. The second panel of Fig. 8 shows a close-up of a portion around the self-intersecting knot. We see there is only one change of signature as we traverse each knot. Fig. 9 shows the distance of the waist to the point where this change hap-

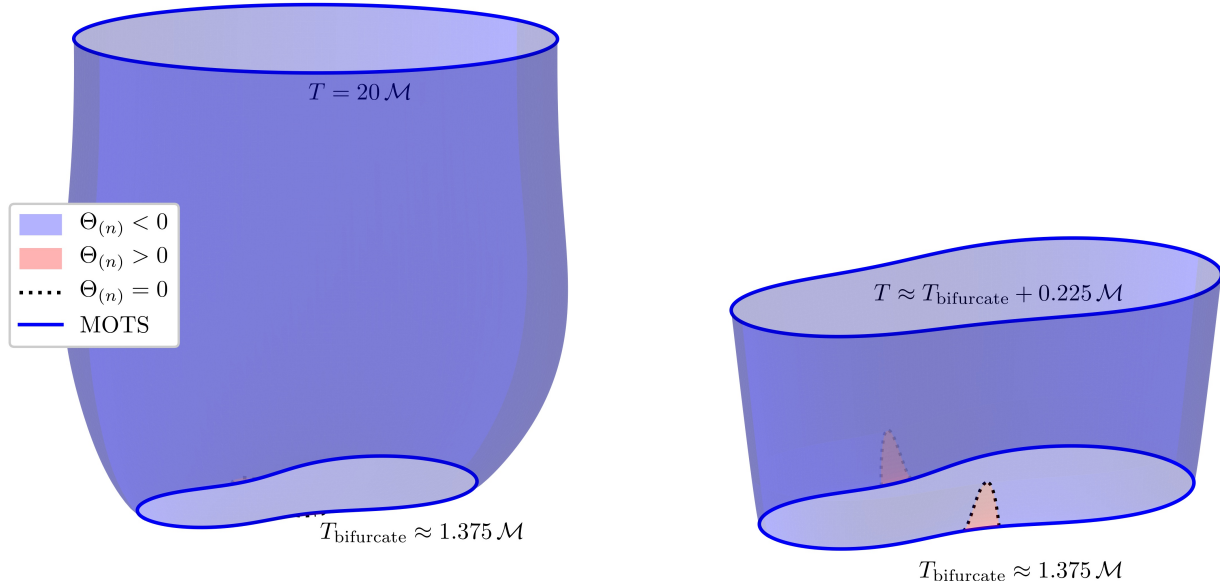


FIG. 5: The sign of $\Theta_{(n)}$ for $\mathcal{H}_{\text{outer}}$. Upon formation, there is a small portion around the waist that has $\Theta_{(n)} > 0$. This portion soon disappears after which time the outer dynamical horizon is a conventional spacelike future-trapped dynamical horizon. The second panel shows a zoom of $\mathcal{H}_{\text{outer}}$ just after it is formed.

pens. The region around the knot is becoming increasingly spacelike.

We can dissect this behavior further in terms of the functions b and c introduced earlier. The apparent horizon at late times is easiest to understand: V^a is spacelike and outward pointing, but strongly tilted towards ℓ^a . Thus, c is small and negative, and b is positive which means that, at late times, the dynamical horizon $\mathcal{H}_{\text{outer}}$ generated by $\mathcal{S}_{\text{outer}}$ must be of type *I*. The same holds for \mathcal{S}_1 and \mathcal{S}_2 at early times. Closer to $T_{\text{bifurcate}}$ when $\mathcal{S}_{\text{outer}}$ is growing rapidly, we must have $b > 0$ and $c < 0$, but c will not be small. The inner horizon is radically different. As it is born, it moves *inwards* rapidly and it is spacelike: it has $b < 0$ and $c > 0$ and is of type *III*. The spacelike portions at early times shown in Fig. 8 (at the bottom of the world tube) are of type *III*. This world tube soon becomes timelike of type *II* wherein $b > 0$ and $c > 0$. This continues till we approach T_{touch} . Shortly before T_{touch} , a part of $\mathcal{S}_{\text{inner}}$ again becomes spacelike: this is the portion which envelops the larger MOTS \mathcal{S}_2 . However, in this spacelike portion it turns out that we have $b > 0$ and $c < 0$, i.e. it is of type *I*. The inner horizon thus shows the following transitions: *III* \rightarrow *II* \rightarrow *I* (partially). It is in fact this spacelike portion of type *I* which is responsible for the anomalous area increase shown in the right panel of Fig. 2.

To explain this, we need to go back to the Bousso-Engelhardt proof of the area increase law [59, 60]. A key intermediate result in this work is Theorem IV.2 of [59] which shows that c cannot change sign. This would seem to rule out the transition *II* \rightarrow *I* described in the pre-

vious paragraph. However, this proof requires the existence of a MOTS which has $c < 0$ everywhere, i.e. it requires that the spacelike portion contains at least one complete MOTS. We see that around T_{touch} , $\mathcal{H}_{\text{inner}}$ has complete MOTSs in the timelike portion, but none in the spacelike portion. Moreover, after T_{touch} , $\mathcal{H}_{\text{inner}}$ violates another requirement assumed in [59, 60], namely that each MOTS should have disjoint “inside” and “outside” regions. Thus, again, there is no contradiction with the proof. Further details can be found in Appendix A. The appendix also shows that a straightforward extension of the proof to our case does not work.

VI. THE ANOMALOUS AREA INCREASE AND THE MEMBRANE PARADIGM

In this final section, we indulge in some speculations on the anomalous area increase. We have mentioned briefly earlier that because of the relation between horizon area and entropy, the anomalous area increase of $\mathcal{H}_{\text{inner}}$ might be physically significant. One approach where this might play a role is in the fluid-gravity correspondence. For black holes in $d + 1$ -dimensional anti-deSitter space, it is suggested in [96] that the area increase law for the event horizon has a dual description in terms of an “entropy current” defined for a relativistic fluid living on the d -dimensional boundary. The calculation presented in [96] is perturbative, where many of the complications of full non-linear general relativity, such as those we have studied, do not arise. In order to extend this correspon-

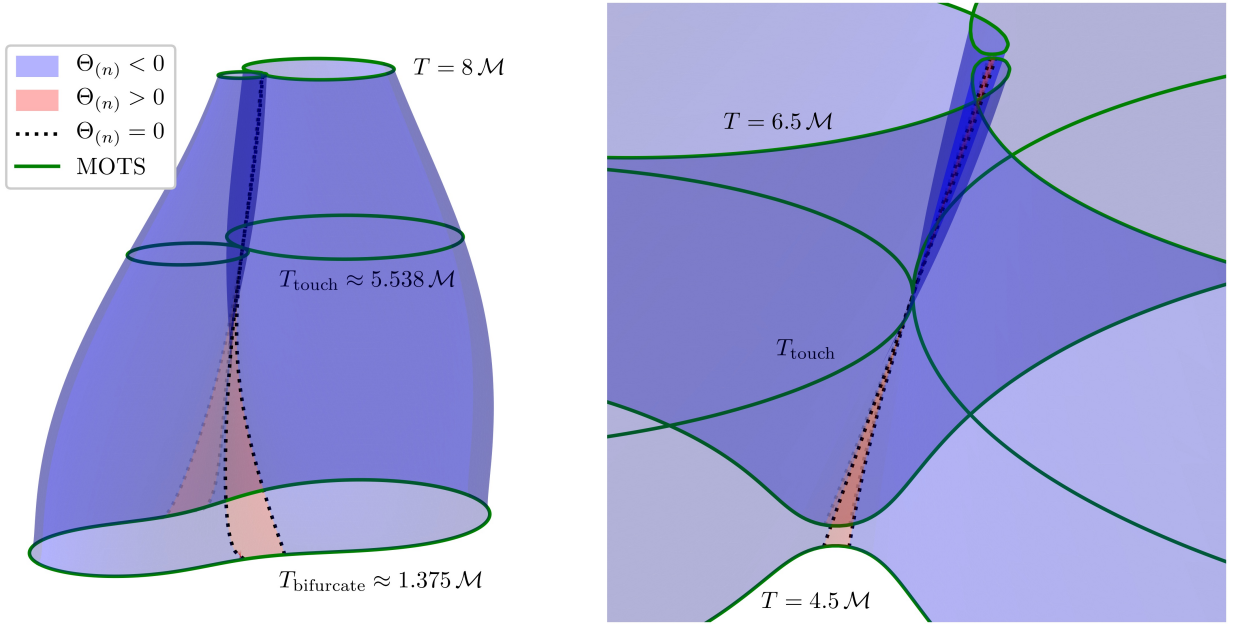


FIG. 6: The sign of $\Theta_{(n)}$ for $\mathcal{S}_{\text{inner}}$. As for the apparent horizon, $\mathcal{S}_{\text{inner}}$ has a portion around its waist with $\Theta_{(n)} > 0$, and this portion becomes smaller over time but does not disappear. The second panel shows details near T_{touch} . We see that the portion with positive $\Theta_{(n)}$ momentarily vanishes at T_{touch} , but reappears again immediately afterwards.

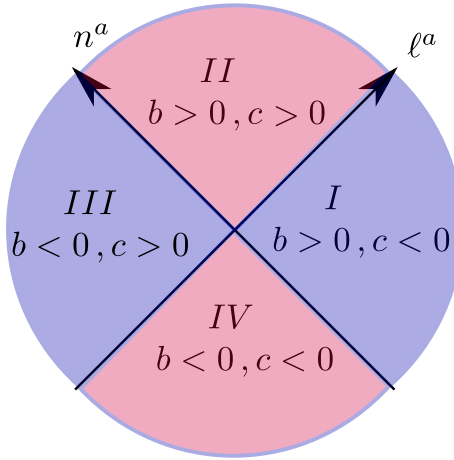


FIG. 7: The four different types of time evolution vector fields on a generic dynamical horizon. The right and left quadrants, *I* and *III* respectively, refer to spacelike dynamical horizons. The top and the bottom quadrants, *II* and *IV* respectively, are timelike. Horizons in the right quadrant are moving outwards while those in the left quadrant move inwards. We do not have any horizons in the bottom quadrant (*IV*) since in our simulations V^a can never be past directed.

dence to non-perturbative situations, it has been argued that the event horizon might not be the appropriate concept, and one should consider dynamical horizons instead [97, 98]. Indeed, because of the teleological and non-local

nature of the event horizon, it would be unusual if its properties could be mapped to a local hydrodynamics description (except in situations where it can be treated perturbatively).

At present, a viable proposal for the dual entropy current for dynamical horizons is lacking. We suggest that binary mergers might provide an interesting test case. If each of the horizons \mathcal{H}_1 and \mathcal{H}_2 at early times have a dual hydrodynamics description and so does the final horizon $\mathcal{H}_{\text{outer}}$ at late times, then the overall increase in area might be viewed as the increase in entropy due to the interaction and mixing between the two fluids. As we have detailed in this paper, the inner horizon $\mathcal{H}_{\text{inner}}$ provides the link between the initial and the final states. Thus, if such a dual description is generally viable then $\mathcal{H}_{\text{inner}}$, and in particular the quantity $c\Theta_{(n)}$ appearing in Eq. (20), is likely to play an important role. The product $c\Theta_{(n)}$ yields the time derivative of the area according to Eq. (20) averaged over the horizons:

$$\oint_S \mathcal{L}_V \tilde{\epsilon} = \dot{A}_S = \oint_S c\Theta_{(n)} dA. \quad (21)$$

The integrals of $c\Theta_{(n)}$ as functions of time for \mathcal{H}_1 , \mathcal{H}_2 and $\mathcal{H}_{\text{outer}}$ are shown in Fig. 10 and these are consistent with Fig. 2. Similarly, Fig. 11 for the inner horizon is consistent with the right panel of Fig. 2; the minimum of the area in the right panel of Fig. 2 is consistent with the zero of $\int c\Theta_{(n)}$ in Fig. 11. While these results are guaranteed mathematically, it is still a useful numerical check since Eq. (21) is an independent calculation of \dot{A}_S .

There exists in fact a different description of a black

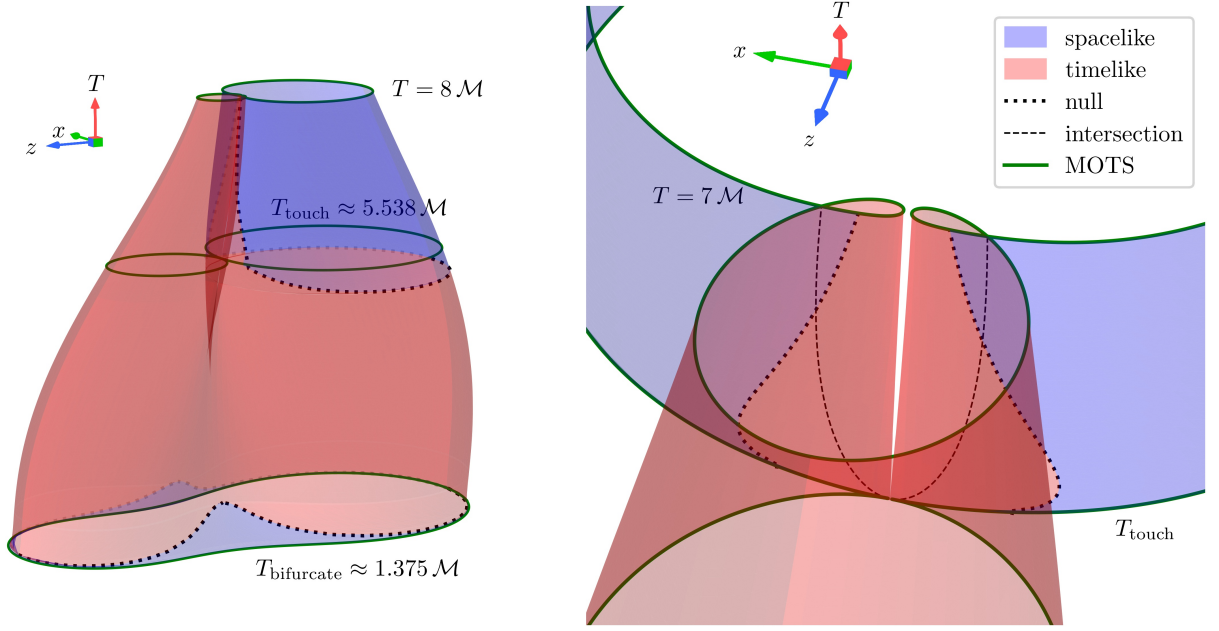


FIG. 8: The signature of the inner-horizon $\mathcal{H}_{\text{inner}}$. Blue shows the spacelike portions and red is timelike. The null portions where the horizon transitions between spacelike and timelike are shown as dotted lines. Upon formation (at $T_{\text{bifurcate}}$) $\mathcal{H}_{\text{inner}}$ is entirely spacelike. This phase however lasts for a very short time (and is not easy to make out in the figure). It develops timelike portions and soon becomes fully timelike. The portions around the “waist” persist in remaining spacelike for the longest. At a later time, a little bit before T_{touch} , the part of $\mathcal{H}_{\text{inner}}$ surrounding the larger black hole reverts to being spacelike. The right panel shows details near the self-intersection. The thin dashed curve is the location of the self-intersection.

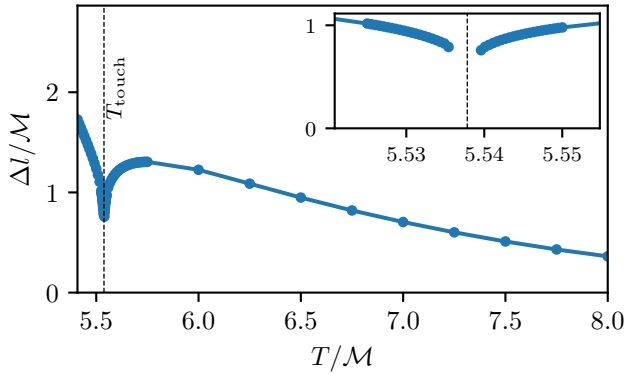


FIG. 9: Proper length Δl of the curve segment connecting the waist of $\mathcal{S}_{\text{inner}}$ to the point where the signature changes from timelike to spacelike. This corresponds to the proper distance measured along the MOTS when going from the waist to the dotted line in Fig. 8. We cannot numerically resolve whether this signature change happens precisely at the cusp (i.e. $\Delta l = 0$) when $T = T_{\text{touch}}$.

hole horizon in terms of fluids, namely that arising in the membrane paradigm mentioned in Sec. II C. As men-

tioned there, the analogy between fields on black hole horizons and a 2-dimensional fluid also works for \mathcal{H} . One of these quantities is the energy density which, it turns out, is proportional to the expansion of V^a . Since $\Theta_{(V)} = c\Theta_{(n)}$, we see that the energy density is proportional to $c\Theta_{(n)}$. The interpretation of $c\Theta_{(n)}$ as an energy density means that $\mathcal{S}_{\text{inner}}$ has large negative energy when it is formed, and its energy becomes positive after T_{min} .

To explain this more fully, we revisit the discussion of the quasi-local membrane paradigm in [88–90], adapting it to MOTTs of arbitrary signature. Given a hypersurface \mathcal{H} , we introduce the orthogonal vector W^a (compare with V^a in Eq. (18))

$$W^a = b\ell^a - cn^a, \quad (22)$$

satisfying $V \cdot W = 0$, $W \cdot W = 2bc = -V \cdot V$. The evolution of its expansion $\Theta_{(W)} = b\Theta_{(\ell)} - c\Theta_{(n)}$ along \mathcal{H} is written as (cf. e.g. [45, 99])

$$\begin{aligned} \mathcal{L}_V \Theta_{(W)} = & \kappa^{(V)} \Theta_{(V)} - \frac{1}{2} \Theta_{(V)} \Theta_{(W)} - \sigma_{ab}^{(V)} \sigma_{ab}^{(W)} \\ & - G_{ab} V^a W^b + (\mathcal{L}_V b) \Theta_{(\ell)} - (\mathcal{L}_V c) \Theta_{(n)} \\ & + \mathcal{D}^a (b \mathcal{D}_a c - c \mathcal{D}_a b - 2bc \omega_a), \end{aligned} \quad (23)$$

where $\kappa^{(V)} = -n^b V^a \nabla_a \ell_b$, $\sigma_{ab}^{(V)} = b\sigma_{ab}^{(\ell)} + c\sigma_{ab}^{(n)}$, $\sigma_{ab}^{(W)} = b\sigma_{ab}^{(\ell)} - c\sigma_{ab}^{(n)}$ and G_{ab} is the Einstein tensor. First we

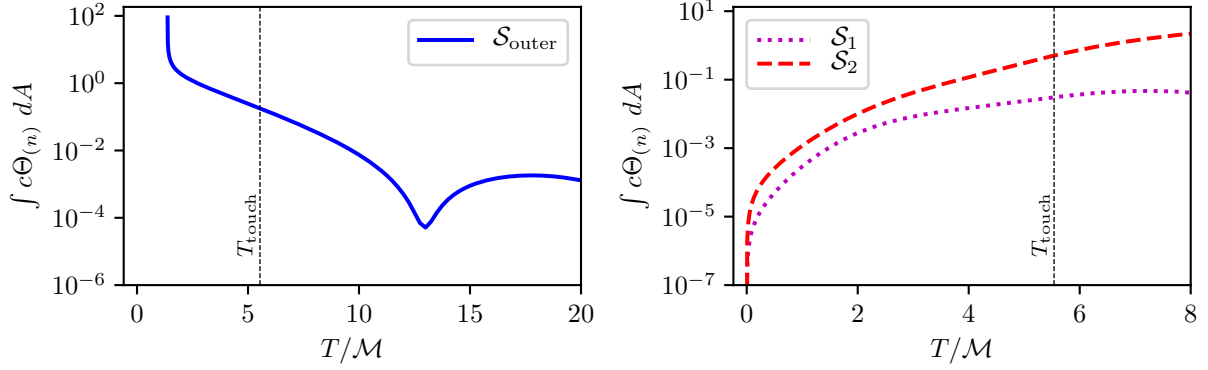


FIG. 10: Plot of the integral of $c\Theta_{(n)}$ as a function of time for $\mathcal{S}_{\text{outer}}$ (left panel) and $\mathcal{S}_1, \mathcal{S}_2$ (right panel), on a logarithmic scale. As explained in the text, this quantity is essentially the rate of change of the area. As expected, and consistent with Fig. 2, this shows that the area of $\mathcal{S}_{\text{outer}}$ increases rapidly on formation (just after $T_{\text{bifurcate}}$) and then settles down. The dip near $\sim 13M$ will be explained in paper II. The individual horizons \mathcal{S}_1 and \mathcal{S}_2 show the opposite behavior, i.e. increasing rapidly only as T_{touch} is approached.

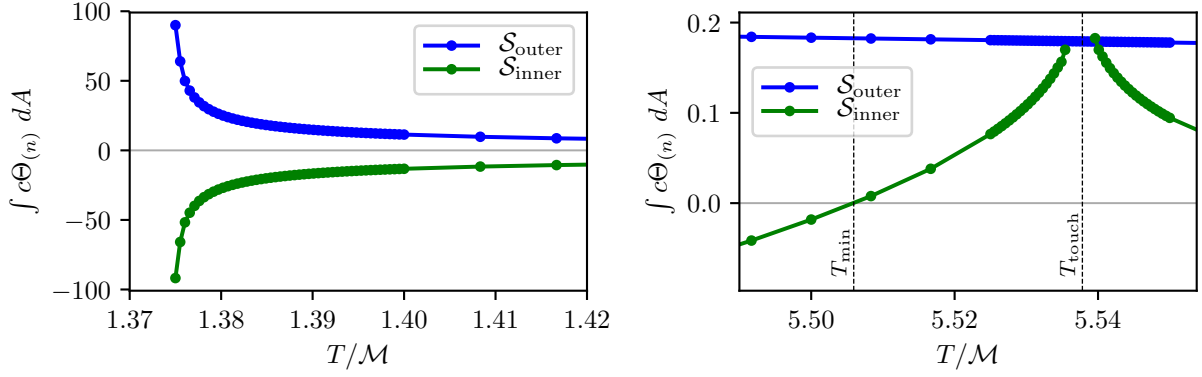


FIG. 11: Plot of the integral of $c\Theta_{(n)}$ for the inner horizon $\mathcal{S}_{\text{inner}}$. The left panel shows the values just after $T_{\text{bifurcate}}$ when $\mathcal{S}_{\text{inner}}$ is formed and rapidly decreases in area, while the right panel shows values near T_{touch} . The results are consistent with the area results. In particular, as we see from the second panel of Fig. 2, the area of $\mathcal{S}_{\text{inner}}$ has a minimum at T_{min} . In the second panel of this plot, we get a zero at T_{min} , consistent with it being the rate of change of the area.

note that, if \mathcal{H} is a smooth event horizon (so in particular a null hypersurface), by making $b = 1$, $c = 0$ so that $V^a = W^a = \ell^a$, we immediately recover the null Raychaudhuri equation. This equation was interpreted by Price and Thorne in [86, 87] as an energy balance law by introducing the surface energy density $\varepsilon = -\Theta_{(W)}/8\pi = -\Theta_{(\ell)}/8\pi$. For a dynamical horizon, namely with $\Theta_{(\ell)} = 0$ and thus $\Theta_{(W)} = -\Theta_{(V)}$, we can write

$$\begin{aligned} \mathcal{L}_V \Theta_{(V)} + \Theta_{(V)}^2 &= -\kappa^{(V)} \Theta_{(V)} + \frac{1}{2} \Theta_{(V)}^2 + \sigma_{ab}^{(V)} \sigma_{(W)}^{ab} \\ &+ G_{ab} V^a W^b + (\mathcal{L}_V \ln c) \Theta_{(V)} \\ &+ \mathcal{D}^a (c \mathcal{D}_a b - b \mathcal{D}_a c + 2bc \omega_a). \end{aligned} \quad (24)$$

Identifying again $\varepsilon = -\Theta_{(W)}/8\pi$ as a formal surface energy density, that in the MOTT case translates into $\varepsilon = \Theta_{(V)}/8\pi = c\Theta_{(n)}/8\pi$, we can interpret \dot{A} in Eq. (21)

in terms of a total surface energy \mathcal{E}

$$\mathcal{E} = \oint_S \varepsilon \tilde{\epsilon} = \frac{1}{8\pi} \oint_S \Theta_{(V)} \tilde{\epsilon} = \frac{1}{8\pi} \oint_S c\Theta_{(n)} \tilde{\epsilon} = \frac{\dot{A}_S}{8\pi}. \quad (25)$$

The rate of change of \mathcal{E}

$$\dot{\mathcal{E}} = \frac{\ddot{A}_S}{8\pi} = \oint_S \mathcal{L}_V (\varepsilon \tilde{\epsilon}) = \oint_S (\mathcal{L}_V \varepsilon + \Theta_{(V)} \varepsilon) \tilde{\epsilon}, \quad (26)$$

is controlled by Eq. (24). This can be cast as an energy balance law

$$\begin{aligned} \mathcal{L}_V \varepsilon + \Theta_{(V)} \varepsilon &= - \left(\frac{\kappa^{(V)}}{8\pi} \right) \Theta_{(V)} + \Theta_{(V)} \left(\frac{\Theta_{(V)}}{16\pi} \right) \\ &+ \sigma_{ab}^{(V)} \left(\frac{\sigma_{(W)}^{ab}}{8\pi} \right) + \Pi - \mathcal{D}_a Q^a, \end{aligned} \quad (27)$$

where $\kappa^{(V)}/8\pi$ is a surface tension (2-dimensional pressure term), $\Theta_{(V)}$ is the fluid expansion (so that a bulk

viscosity coefficient $\zeta = 1/16$ can be identified), $\sigma_{ab}^{(V)}$ and $\sigma_{ab}^{(W)}/8\pi$ are, respectively, the shear strain and stress tensors (in general not proportional, so MOTTs do not correspond to Newtonian fluids and therefore a shear viscosity μ cannot be defined), $\Pi := T_{ab}V^aW^b + \frac{1}{8\pi}(\mathcal{L}_V \ln c)\Theta_{(V)}$ is an external energy production rate (enforced by the Einstein equations) and $Q^a := (b\mathcal{D}^a c - c\mathcal{D}^a b - 2bc\omega^a)/8\pi$ is heat flux.

This fluid description arising in the membrane paradigm is however only a formal analogy. There is, unlike in the fluid-gravity correspondence, no deeper interpretation in terms of any dual boundary description or otherwise. Nevertheless, it is still interesting that the analogy goes through for the inner horizon as well. In Appendix B, we show that the analogy also extends to spinning black holes, i.e. to include the rotation 1-form ω_a , which serves to define a momentum density on \mathcal{H} . We shall make further use of this analogy in paper II. In particular following [100, 101] in this viscous fluid picture, the evolution equation for $\Theta_{(V)}$ will be employed to introduce decay and oscillation timescales leading to a slowness parameter [102] for the approach of a dynamical horizon to equilibrium.

VII. CONCLUSIONS

In this paper we have studied geometrical properties of the world tube of marginally outer trapped surfaces in a binary black hole merger. This includes the status of the area increase law, and the different ingredients which go into the rate of change of the area, i.e. the expansion of the ingoing null normal $\Theta_{(n)}$ and the signature of the world tube. We have seen that the horizons are of mixed signature with various transitions between spacelike and timelike portions, especially for the inner horizon. Cross-sections of the inner horizon can be of mixed signature. Similarly, the condition $\Theta_{(n)} < 0$ is not satisfied everywhere for the inner horizon. The anomalous area increase apparently contradicts existing proofs of the area increase law, in particular the Bousso-Engelhardt result. We have argued that technical assumptions required for this proof do not hold in our case. We have briefly discussed the anomalous area increase in terms of the membrane-paradigm analogy using the energy density of a fictitious 2-dimensional fluid. The deeper physical significance of the anomalous area increase, if any, is still not understood.

The second paper will continue this study and consider physical quantities such as energy fluxes, multipole moments and the stability operator on all of these horizons.

ACKNOWLEDGMENTS

We are indebted to Abhay Ashtekar, Ivan Booth and Ricardo Uribe-Vargas for valuable discussions and suggestions. Research at Perimeter Institute is supported

in part by the Government of Canada through the Department of Innovation, Science and Economic Development Canada and by the Province of Ontario through the Ministry of Colleges and Universities. We also thank the French EIPHI Graduate School (ANR-17-EURE-0002) and the Spanish FIS2017-86497-C2-1 project (with FEDER contribution) for support.

Appendix A: Comparison with the Bousso-Engelhardt area increase law

In this Appendix, we show that the anomalous area increase does not violate any of the existing proofs of the area increase laws. The most general proof to-date is due to Bousso & Engelhardt [59, 60], and an extension thereof due to Sanches & Weinberg [61]. These proofs formally apply to future dynamical horizons, or holographic screens in the terminology of [59, 60]. We note that this proof is in fact an application of the maximum principle for elliptic operators. The application of the maximum principle to null-surfaces was studied previously by Galloway [103]. These methods have previously been applied by Ashtekar & Galloway to spacelike dynamical horizons to show e.g. the uniqueness of the foliation by MOTSs [58]. We shall discuss the proof in more detail below, but roughly speaking, these results would naively indicate that the inner horizon should have decreasing area and would seem to rule out the anomalous area increase. While these results assume $\Theta_{(n)} < 0$, this is only a sufficient but not necessary condition. The regions on the horizon with $\Theta_{(n)} > 0$ are small near T_{touch} and do not, by themselves, explain the area increase. In other words, we can split the area (and similarly also its rate of change) as the sum of two terms depending on the sign of $\Theta_{(n)}$:

$$A_S = \int_{\Theta_{(n)} < 0} dA + \int_{\Theta_{(n)} > 0} dA. \quad (\text{A1})$$

The area over the $\Theta_{(n)} < 0$ portion turns out to be much larger than the second term, and it has a correspondingly larger effect on \dot{A}_S . We saw for example that the area of $\mathcal{S}_{\text{outer}}$ increases as expected despite it not having $\Theta_{(n)} < 0$ everywhere.

The difficulty, and apparent contradiction, lies elsewhere. It is the spacelike portion on the inner horizon near T_{touch} that leads to the anomalous area increase. A key ingredient of the Bousso-Engelhardt results is an intermediate step showing that the function c is not allowed to change sign. Thus, if we actually had $\Theta_{(n)} < 0$, then $c\Theta_{(n)}$ cannot change sign, and the area increase law follows directly from Eq. (20) (it must increase with time for regions *I* and *IV*, and decrease with time for regions *II* and *III*). In the transition from timelike to spacelike of the inner horizon near T_{touch} , which we have seen is a transition *II* \rightarrow *I* of Fig. 7, this is precisely what goes wrong: c goes from positive to negative. Moreover, this intermediate result only uses the condition $\Theta_{(\ell)} = 0$ and

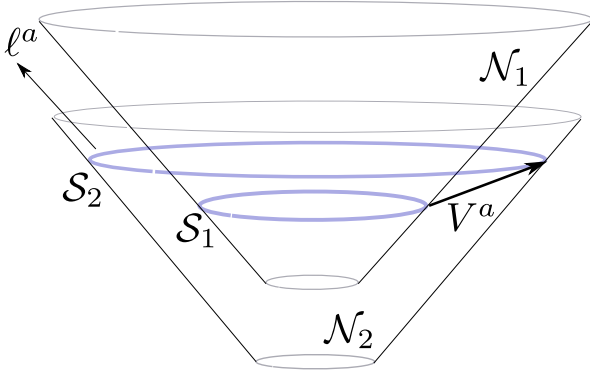


FIG. 12: As a MOTS evolves in a spatially outward direction from \mathcal{S}_1 to \mathcal{S}_2 , the null surface \mathcal{N}_2 is nowhere to the future of \mathcal{N}_1 .

does not rely upon $\Theta_{(n)} < 0$. So how can this intermediate result be consistent with the results of this paper? To understand this we need to delve into some of the technical conditions required in the Bousso-Engelhardt proof. We shall not spell out the details of the proof, but we instead offer a pictorial description which will make the result plausible.

The simplest case which we sketch here is the proof that the transition $I \rightarrow II$ is ruled out. We thus start out with a MOTS evolving spatially outward, which later partially switches over to a future timelike direction. For a MOTS \mathcal{S} , we construct the outgoing null surface \mathcal{N} generated by the null-rays starting from ℓ^a . Denote the part of \mathcal{N} to the future of \mathcal{S} by \mathcal{N}^+ , and the portion to the past by \mathcal{N}^- . If we move \mathcal{S}_1 spatially outwards along V^a to a new MOTS \mathcal{S}_2 , the null surface \mathcal{N}_2 is easily seen to be nowhere to the future of \mathcal{N}_1 ; see Fig. 12. If V^a partially changes to a future timelike direction, this will eventually cease to hold.

Consider now the dynamical horizon, i.e. the world tube spanned by \mathcal{S} as it evolves along V^a . Let the part of \mathcal{H} with $c > 0$ be denoted as \mathcal{H}^+ , the part with $c < 0$ as \mathcal{H}^- , and the part with $c = 0$ as \mathcal{H}^0 . Assume that \mathcal{H} has initially a leaf completely of type I , i.e. we assume $c < 0$ on a complete leaf. Let λ be the affine parameter along V^a , i.e. $V^a \partial_a \lambda = 1$, and let $\lambda = \lambda_0$ at the initial MOTS \mathcal{S}_{λ_0} (which has $c < 0$).

Let us take \mathcal{H}^+ to lie in the $\lambda > \lambda_0$ region; this will be shown to lead to a contradiction. Let $\lambda_1 > \lambda_0$ be the smallest value of λ on \mathcal{H}^+ , i.e. when the timelike portion first appears. Clearly, \mathcal{N}_{λ_1} lies nowhere to the future of \mathcal{N}_{λ_0} . We can move further infinitesimally to $\lambda_1 + \epsilon$ still without entering the future of \mathcal{N}_{λ_0} . Consider then the MOTS $\mathcal{S}_{\lambda_1+\epsilon}$ and its subset $\mathcal{S}^+ = \mathcal{S}_{\lambda_1+\epsilon} \cap \mathcal{H}^+$. Then trace back the null rays to the past along \mathcal{N}^- , and let k^a denote the null generator of \mathcal{N}^- . Let us follow \mathcal{N}^- back in time and look at its intersection with Cauchy surfaces corresponding to various values of $\lambda < \lambda_1$. The intersection $\mathcal{N}^- \cap \mathcal{H}$ is generically a curve on \mathcal{H} . Let the minimum value of λ on this intersection be denoted λ^* .

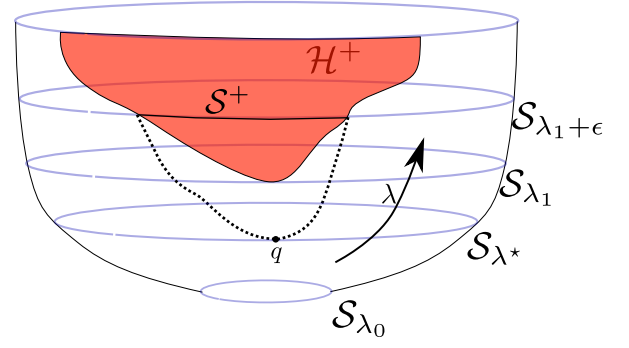


FIG. 13: A pictorial sketch of the Bousso-Engelhardt proof. The portion of \mathcal{H} with the offending timelike region of type II with $c > 0$ is \mathcal{H}^+ . The rest of the horizon is of type I . The parameter λ increases upwards. \mathcal{S}_{λ_0} is the MOTS at λ_0 , and λ_1 is the earliest that \mathcal{H}^+ appears. \mathcal{S}^+ is the portion of $\mathcal{S}_{\lambda_1+\epsilon}$ within \mathcal{H}^+ . The dashed curve depicts the intersection of \mathcal{H} with the null surface \mathcal{N}^- (generated by the past-inward directed null curves along $-\ell^a$ starting from \mathcal{S}^+). The point q is where λ has a minimum over the dashed curve. At q , the null generator of the \mathcal{N}^- coincides with the outgoing null normal of the MOTS \mathcal{S}_{λ^*} which is, by definition, supposed to have vanishing expansion.

Since ϵ is chosen sufficiently small, \mathcal{N}^- lies to the past of \mathcal{S}_{λ_0} so that $\lambda^* > \lambda_0$. Let $q \in \mathcal{S}_{\lambda^*}$ be the point where the minimum is achieved. This construction is shown pictorially in Figs. 13 and 14. Fig. 13 depicts the world tube, its timelike portion, and the intersection with \mathcal{N}^- . The same situation is shown in Fig. 14 in terms of how these surfaces would appear on Cauchy surfaces at various times.

Then, it can be shown that \mathcal{N}^- is tangent to \mathcal{S}_{λ^*} ; they share the same null normal at q so that by a suitable rescaling we can set $k^a = \ell^a$ at q . However, since \mathcal{S}_{λ^*} is “inside” \mathcal{N}^- , it has larger curvature, and thus we must have $\Theta_{(\ell)}(q) \geq \Theta_{(k)}(q)$ where $\Theta_{(k)}(q)$ is the expansion of k^a at q . From the Raychaudhuri equation, and assuming the null energy condition and the positivity of $|\sigma^{(k)}|^2$, it follows that $\Theta_{(k)}(q) > 0$. This implies then that $\Theta_{(\ell)}(q) \geq \Theta_{(k)}(q) > 0$ which contradicts $\Theta_{(\ell)}(q) = 0$ (the defining condition for a MOTS). Thus, \mathcal{H}^+ cannot exist and the transition $I \rightarrow II$ is ruled out.

A similar argument, works for the transition from region $II \rightarrow I$, except we follow the null surface to the future, and it is required to have a complete MOTS with $c < 0$. The other forbidden transitions where c changes sign are $IV \rightarrow III$ and $III \rightarrow IV$. In both of these cases, a direct attempt at applying the above argument does not work. Instead, one needs to reverse the direction of V so that these are reduced to the previous two cases.

The details of this proof are given in [59, 60]; see also [58, 103]. Here we list the technical conditions and Lemmas which must hold for the above argument to go through:

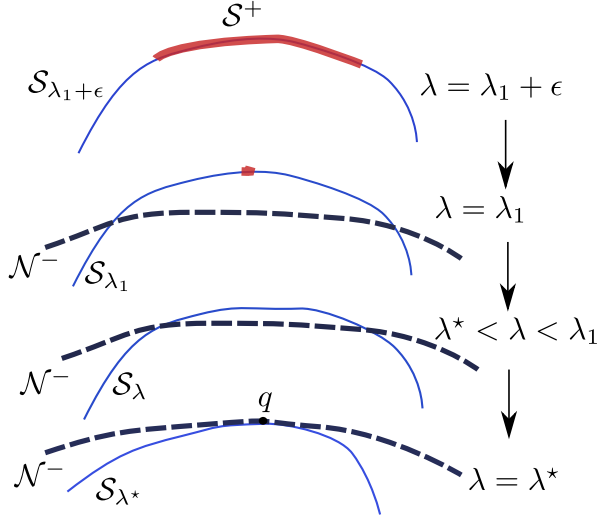


FIG. 14: Same as Fig. 13, but now showing how the various surfaces would appear on Cauchy surfaces. We start with $\lambda_1 + \epsilon$ where we start tracing back \mathcal{N}^- . The color scheme is consistent with Fig. 13: the portion in red is the timelike portion \mathcal{S}^+ , the blue curve the MOTS, while the dashed curve shows the intersection of \mathcal{N}^- with the Cauchy surfaces. The timelike portion will contract slower than the null surface, and will thus stay outside the null portion. Eventually, at λ^* , the intersection is the point q . \mathcal{S}_{λ^*} is tangent to \mathcal{N}^- at q , and the rest of it lies “inside” \mathcal{N}^- . The maximum principle is applied in a neighborhood of q .

1. Each MOTS \mathcal{S}_λ which foliate \mathcal{H} must have an “inside” and an “outside”, i.e. if they lie on a Cauchy surface Σ , they must split it into two disjoint portions.
2. The existence of a MOTS \mathcal{S}_0 which has $c < 0$ everywhere – required for the point q which minimizes λ to exist.
3. Genericity condition on the zeros of b and c , $\partial\mathcal{H}^+ = \mathcal{H}^0 = \partial\mathcal{H}^-$ – this excludes non-generic zeros of c or b (e.g. the zeros must not coincide with extrema, and the functions cannot vanish in an open set).
4. On any \mathcal{S} , $|\sigma|^2$ must be positive definite (in the presence of matter, we would include the null energy condition) – this ensures the positivity of $\Theta_{(k)}(q)$.
5. The proof of $\Theta_{(\ell)}(q) \geq \Theta_{(k)}(q)$ is given in [104]; see [103] for a more general proof with, e.g. weaker smoothness assumptions, explicitly using the maximum principle.

All of these conditions do hold on $\mathcal{S}_{\text{outer}}$, \mathcal{S}_1 and \mathcal{S}_2 but not on $\mathcal{S}_{\text{inner}}$ where the first two are violated. (1) is violated by the self intersecting MOTSs but this only happens after T_{touch} and is not relevant for the anomalous

area increase which occurs *before* T_{touch} . The culprit is then condition (2): We see that near T_{touch} , we have $c < 0$ only over a part of the MOTSs before T_{touch} . Thus, the proof of [59, 60] does not rule out the anomalous area increase scenario presented above. Repeating the proof by dropping the requirement of a complete MOTS with $c < 0$, and replacing it with requiring that there should be a complete MOTS in region *II* (as is the case here) is seen to not work either.

To show this, let us look explicitly at the case of interest to us, namely a transition $II \rightarrow I$ (future-timelike to outward-spacelike). The transition is partial and we do not have any section which is entirely spacelike. We do however have a complete MOTS in the timelike portion. The picture is very similar to Fig. 13, with the timelike and spacelike portions interchanged. Thus, \mathcal{H}^+ becomes \mathcal{H}^- and \mathcal{S}^+ can be labeled \mathcal{S}^- . Similarly, Fig. 14 can be reused but with the curves for \mathcal{N}^- and the various \mathcal{S} interchanged. Since \mathcal{S}^- is spacelike, it contracts faster than \mathcal{N}^- , and thus it goes inside \mathcal{N}^- . At λ^* , we again have \mathcal{N}^- tangent to \mathcal{S}_{λ^*} , but critically, \mathcal{S}_{λ^*} now lies “outside” \mathcal{N}^- . Thus, while we still have $\Theta_{(k)}(q) > 0$, but now $\Theta_{(\ell)}(q) \leq \Theta_{(k)}(q)$, and no contradiction arises with $\Theta_{(\ell)}(q) = 0$.

Appendix B: Damour-Navier-Stokes equation in MOTTs

For completeness, in the context of the quasi-local membrane paradigm discussed in section VI, we present here the equation for the evolution of the rotation form ω_a , interpreted as a (Damour)-Navier-Stokes equation for the momentum density of the two-dimensional fluid.

As we did for $\Theta_{(V)}$, we evaluate now the evolution of ω_a along a hypersurface \mathcal{H}

$$\begin{aligned} \mathcal{L}_V \omega_a + \Theta_{(V)} \omega_a &= \mathcal{D}_a \kappa^{(V)} + \frac{1}{2} \mathcal{D}_a \Theta_{(V)} - \mathcal{D}_b \sigma^{(W)b}_a (B1) \\ &+ q_a {}^b G_{bc} W^c - \Theta_{(\ell)} \mathcal{D}_a b + \Theta_{(n)} \mathcal{D}_a c. \end{aligned}$$

Making first $b = 1$ and $c = 0$, i.e. $V^a = W^a = \ell^a$, we recover the evolution equation of the rotation form on a null hypersurface [21], in particular the one satisfied on a general (smooth) event horizon

$$\begin{aligned} \mathcal{L}_V \omega_a + \Theta_{(\ell)} \omega_a &= \mathcal{D}_a \kappa^{(\ell)} + \frac{1}{2} \mathcal{D}_a \Theta_{(\ell)} - \mathcal{D}_b \sigma^{(\ell)b}_a \\ &+ q_a {}^b G_{bc} W^c. \end{aligned} \quad (B2)$$

Following Damour [84, 85], this equation can be interpreted as a Navier-Stokes equation by defining a momentum surface density $\pi_a = -\omega_a/8\pi$, leading to a Newtonian viscous fluid picture with negative bulk viscosity $\zeta = -1/16\pi$ and shear viscosity $\mu = 1/16\pi$. In our MOTT case, making $\Theta_{(\ell)} = 0$ in Eq. (B1), we get

$$\begin{aligned} \mathcal{L}_V \omega_a + \Theta_{(V)} \omega_a &= \mathcal{D}_a \kappa^{(V)} + \frac{1}{2} \mathcal{D}_a \Theta_{(V)} - \mathcal{D}_b \sigma^{(W)b}_a \\ &+ q_a {}^b G_{bc} W^c + \Theta_{(V)} \mathcal{D}_a \ln c. \end{aligned} \quad (B3)$$

Defining, as in the event horizon case, a momentum surface density $\pi_a = -\omega_a/8\pi$ we get [88]

$$\begin{aligned} \mathcal{L}_V \pi_a + \Theta_{(V)} \pi_a = & -\mathcal{D}_a \left(\frac{\kappa^{(V)}}{8\pi} \right) + \mathcal{D}_a \left(\frac{\Theta_{(V)}}{16\pi} \right) \\ & + \mathcal{D}_b \left(\frac{\sigma_a^{(W)b}}{8\pi} \right) + f_a, \end{aligned} \quad (\text{B4})$$

that corresponds to a viscous fluid with the interpretation of the terms given after Eq. (27), namely a Newtonian fluid in the trace part of the viscous stress tensor (since it is proportional to the trace of the strain tensor, i.e. the expansion $\Theta_{(V)}$) with positive bulk viscosity $\zeta = 1/16\pi$, non-Newtonian in the shear stress tensor part (since $\sigma_{ab}^{(W)}/8\pi$ is not in general proportional to the strain shear tensor $\sigma_{ab}^{(V)}$). The term $f_a := -q_a{}^b T_{bc} W^c - \frac{1}{8\pi} \Theta_{(V)} \mathcal{D}_a \ln c$, where Einstein equations are imposed, corresponds to an external force surface density¹. See [105] for a critical account of this viscous fluid interpretation.

Equations (B1) and (B4) are valid for general signature MOTTs, where V^a can be proportional n^a . In contrast with the $\Theta_{(V)}$ evolution and the energy balance equation discussed in section VI, where the “heat flux” term Q^a must be generalized, Eqs. (B1) and (B4) coincide exactly with those in [88–90], that were originally restricted to deviations around the outgoing null vector ℓ^a .

Appendix C: Contact structures: a tentative bridge from immersed MOTS to wavefronts and caustics

As observed in Fig. 8 and fully discussed in Section VI of [27], the inner common horizon $\mathcal{S}_{\text{inner}}$ transitions from i) a smooth “embedded curve” before time T_{touch} , into ii) a singular curve (vanishing of its differential) with cusps at T_{touch} , and then to iii) an “immersed curve” with self-intersections (knot) after T_{touch} . In a complementary view to this “parametrised curve” perspective, we could approach such a sequence in terms of projections: the

described transition corresponds indeed to the generic curve metamorphoses (“perestroikas”) happening when projecting a three-dimensional curve into a plane with the projection direction changing with a parameter [106]. Indeed, as illustrated in [17], such self-intersections seem to have a “genericity” flavor in trapped regions.

Such a projection view suggests a picture with the “lifted” curve as the fundamental object and self-intersections as an artifact of the projections. The natural question is: what is the appropriate higher-dimensional space in which MOTSs “truly” live? A suggestive tentative answer is given in terms of contact structures [107, 108].

Specifically, and dwelling now beyond axisymmetry, let us consider a n -dimensional spacetime \mathcal{M} and its cotangent bundle $T^*\mathcal{M}$ with natural Liouville form $\Lambda = p_a dx^a$. After removing the vanishing one-forms, $T^*\mathcal{M} \setminus \{0_M^*\}$, we can take quotient by one-form rescalings with non-vanishing real numbers \mathbb{R}^* . The resulting space $PT^*\mathcal{M} = (T^*\mathcal{M} \setminus \{0_M^*\})/\mathbb{R}^*$ is the “projectified cotangent bundle”. Crucially, at each point, the kernel of Λ is invariant under such \mathbb{R}^* -rescalings and projects onto hyperplanes in the tangent space of $PT^*\mathcal{M}$: such field of (non-integrable) hyperplanes defines a “contact structure” on $PT^*\mathcal{M}$. In a local chart (x^a, p_a) , with say $p_n \neq 0$, we can consider the “affine” chart (x^i, p_i, z) , $i \in \{1, \dots, n-1\}$ with $z = x^n, p_n = 1$. Then $\Lambda' = p_i dx^i + dz$ is the contact form of the $(2n-1)$ -contact manifold $PT^*\mathcal{M}$ (cf. [108] for a discussion in a general relativistic setting; see also [109]).

The relevance of such contact structures is that they rule the properties of light propagation in the geometric optics approximation, in particular the geometry of light wavefronts and the formation of caustics [110]. In this sense, and given the constitutive relation between (marginally) trapped surfaces and light convergence, such a higher-dimensional geometry seems a promising setting in which lifts of spacetime MOTSs could exist as embedded, properly not self-intersecting, surfaces. Elucidating their ultimate relation to wavefronts and caustics could shed light onto the here discussed patterns of MOTS dynamics and the understanding of the trapped region.

-
- [1] Roger Penrose, “Gravitational collapse and space-time singularities,” *Phys. Rev. Lett.* **14**, 57–59 (1965).
 - [2] S. W. Hawking and R. Penrose, “The Singularities of gravitational collapse and cosmology,” *Proc. Roy. Soc. Lond.* **A314**, 529–548 (1970).
 - [3] B.P. Abbott *et al.* (LIGO Scientific, Virgo), “GWTC-

- 1: A Gravitational-Wave Transient Catalog of Compact Binary Mergers Observed by LIGO and Virgo during the First and Second Observing Runs,” *Phys. Rev. X* **9**, 031040 (2019), arXiv:1811.12907 [astro-ph.HE].
- [4] B. P. Abbott *et al.* (LIGO Scientific, Virgo), “Binary Black Hole Mergers in the first Advanced LIGO Observing Run,” *Phys. Rev. X* **6**, 041015 (2016), [erratum: *Phys. Rev. X* **8**, no.3, 039903 (2018)], arXiv:1606.04856 [gr-qc].
- [5] Alexander H. Nitz, Collin Capano, Alex B. Nielsen, Steven Reyes, Rebecca White, Duncan A. Brown, and Badri Krishnan, “1-OGC: The first open gravitational-wave catalog of binary mergers from analysis of public Advanced LIGO data,” *Astrophys. J.* **872**, 195 (2019),

¹ To complete this picture, it is interesting to note that the principal eigenvalue Λ_o of the MOTS stability operator, that will be systematically studied in Paper II, also admits a membrane paradigm interpretation. Namely, it can be seen as the pressure difference at the interphase between two fluids, in the spirit of a Young-Laplace law [47].

- arXiv:1811.01921 [gr-qc].
- [6] Alexander H. Nitz, Thomas Dent, Gareth S. Davies, Sumit Kumar, Collin D. Capano, Ian Harry, Simone Mozzon, Laura Nuttall, Andrew Lundgren, and Merton Tpai, “2-OGC: Open Gravitational-wave Catalog of binary mergers from analysis of public Advanced LIGO and Virgo data,” *Astrophys. J.* **891**, 123 (2019), arXiv:1910.05331 [astro-ph.HE].
 - [7] Tejaswi Venumadhav, Barak Zackay, Javier Roulet, Liang Dai, and Matias Zaldarriaga, “New Binary Black Hole Mergers in the Second Observing Run of Advanced LIGO and Advanced Virgo,” (2019), arXiv:1904.07214 [astro-ph.HE].
 - [8] Barak Zackay, Tejaswi Venumadhav, Liang Dai, Javier Roulet, and Matias Zaldarriaga, “Highly spinning and aligned binary black hole merger in the Advanced LIGO first observing run,” *Phys. Rev. D* **100**, 023007 (2019), arXiv:1902.10331 [astro-ph.HE].
 - [9] R. A. Matzner, H. E. Seidel, Stuart L. Shapiro, L. Smarr, W. M. Suen, Saul A. Teukolsky, and J. Winicour, “Geometry of a black hole collision,” *Science* **270**, 941–947 (1995).
 - [10] Dieter R. Brill and Richard W. Lindquist, “Interaction energy in geometrostatics,” *Phys. Rev.* **131**, 471–476 (1963).
 - [11] Daniel Pook-Kolb, Ofek Birnholtz, Badri Krishnan, and Erik Schnetter, “Existence and stability of marginally trapped surfaces in black-hole spacetimes,” *Phys. Rev. D* **99**, 064005 (2019).
 - [12] P. Mösta, L. Andersson, J. Metzger, B. Szilágyi, and J. Winicour, “The Merger of Small and Large Black Holes,” *Class. Quant. Grav.* **32**, 235003 (2015), arXiv:1501.05358 [gr-qc].
 - [13] Christopher Evans, Deborah Ferguson, Bhavesh Khamesra, Pablo Laguna, and Deirdre Shoemaker, “Inside the Final Black Hole: Puncture and Trapped Surface Dynamics,” (2020), arXiv:2004.11979 [gr-qc].
 - [14] D. Gannon, “Singularities in nonsimply connected space-times,” *J. Math. Phys.* **16**, 2364 (1975).
 - [15] D. Gannon, “On the topology of spacelike hypersurfaces, singularities and black holes,” *Gen. Rel. Grav.* **7**, 219 (1976).
 - [16] Daniel Pook-Kolb, Ofek Birnholtz, Badri Krishnan, and Erik Schnetter, “Interior of a binary black hole merger,” *Phys. Rev. Lett.* **123**, 171102 (2019).
 - [17] Ivan Booth, Robie Hennigar, and Saikat Mondal, “Marginally outer trapped (open) surfaces and extreme mass ratio mergers,” (2020), arXiv:2005.05350 [gr-qc].
 - [18] Sean A. Hayward, “Black holes: New horizons,” in *Recent developments in theoretical and experimental general relativity, gravitation and relativistic field theories. Proceedings, 9th Marcel Grossmann Meeting, MG’9, Rome, Italy, July 2-8, 2000. Pts. A-C* (2000) pp. 568–580, arXiv:gr-qc/0008071 [gr-qc].
 - [19] Ivan Booth, “Black hole boundaries,” *Can. J. Phys.* **83**, 1073–1099 (2005), arXiv:gr-qc/0508107.
 - [20] Abhay Ashtekar and Badri Krishnan, “Isolated and dynamical horizons and their applications,” *Living Rev. Rel.* **7**, 10 (2004), arXiv:gr-qc/0407042.
 - [21] Ericourgoulhon and Jose Luis Jaramillo, “A 3+1 perspective on null hypersurfaces and isolated horizons,” *Phys. Rept.* **423**, 159–294 (2006), arXiv:gr-qc/0503113.
 - [22] Matt Visser, “Black holes in general relativity,” *PoS BHSGRANDSTRINGS2008*, 001 (2008), arXiv:0901.4365 [gr-qc].
 - [23] Jose Luis Jaramillo, “An introduction to local Black Hole horizons in the 3+1 approach to General Relativity,” *Int. J. Mod. Phys. D* **20**, 2169 (2011), arXiv:1108.2408 [gr-qc].
 - [24] S.A. Hayward, *Black Holes: New Horizons*, New horizons (World Scientific, 2013).
 - [25] Valerio Faraoni and Angus Prain, “Understanding dynamical black hole apparent horizons,” *Lecture Notes in Physics* **907**, 1–199 (2015), arXiv:1511.07775 [gr-qc].
 - [26] R.P.A.C. Newman, “Topology and stability of marginal 2-surfaces,” *Class. and Quant. Grav.* **4**, 277–290 (1987).
 - [27] Daniel Pook-Kolb, Ofek Birnholtz, Badri Krishnan, and Erik Schnetter, “Self-intersecting marginally outer trapped surfaces,” *Phys. Rev. D* **100**, 084044 (2019).
 - [28] Daniel Pook-Kolb, Ofek Birnholtz, Badri Krishnan, and Erik Schnetter, “MOTS Finder version 1.1,” (2019), 10.5281/zenodo.2591105.
 - [29] Jonathan Thornburg, “A Fast Apparent-Horizon Finder for 3-Dimensional Cartesian Grids in Numerical Relativity,” *Class. Quant. Grav.* **21**, 743–766 (2004), arXiv:gr-qc/0306056.
 - [30] Jonathan Thornburg, “Event and Apparent Horizon Finders for 3 + 1 Numerical Relativity,” *Living Rev. Rel.* **10**, 3 (2007), arXiv:gr-qc/0512169.
 - [31] Jonathan Thornburg, “Finding apparent horizons in numerical relativity,” *Phys. Rev. D* **54**, 4899–4918 (1996), arXiv:gr-qc/9508014.
 - [32] Deirdre M. Shoemaker, Mijan F. Huq, and Richard A. Matzner, “Generic Tracking of Multiple Apparent Horizons with Level Flow,” *Phys. Rev. D* **62**, 124005 (2000), arXiv:gr-qc/0004062.
 - [33] Lap-Ming Lin and Jerome Novak, “A new spectral apparent horizon finder for 3D numerical relativity,” *Class. Quant. Grav.* **24**, 2665–2676 (2007), arXiv:gr-qc/0702038.
 - [34] Jose Luis Jaramillo, Marcus Ansorg, and Nicolas Vasset, “Application of initial data sequences to the study of black hole dynamical trapping horizons,” *Physics and mathematical of gravitation. Proceedings, Spanish Relativity Meeting, Salamanca, Spain, September 15-19, 2008*, AIP Conf. Proc. **1122**, 308–311 (2009), arXiv:1103.6180 [gr-qc].
 - [35] Frank Löffler, Joshua Faber, Eloisa Bentivegna, Tanja Bode, Peter Diener, Roland Haas, Ian Hinder, Bruno C. Mundim, Christian D. Ott, Erik Schnetter, Gabrielle Allen, Manuela Campanelli, and Pablo Laguna, “The Einstein Toolkit: A Community Computational Infrastructure for Relativistic Astrophysics,” *Class. Quantum Grav.* **29**, 115001 (2012), arXiv:1111.3344 [gr-qc].
 - [36] EinsteinToolkit, “Einstein Toolkit: Open software for relativistic astrophysics,” <http://einstein toolkit.org/>.
 - [37] Marcus Ansorg, Bernd Brügmann, and Wolfgang Tichy, “A single-domain spectral method for black hole puncture data,” *Phys. Rev. D* **70**, 064011 (2004), arXiv:gr-qc/0404056.
 - [38] Marcus Ansorg, “Double-domain spectral method for black hole excision data,” *Phys. Rev. D* **72**, 024018 (2005), arXiv:gr-qc/0505059 [gr-qc].
 - [39] J. David Brown, Peter Diener, Olivier Sarbach, Erik Schnetter, and Manuel Tiglio, “Turduckening black holes: an analytical and computational study,” *Phys. Rev. D* **79**, 044023 (2009), arXiv:0809.3533 [gr-qc].

- [40] Sascha Husa, Ian Hinder, and Christiane Lechner, “Kranc: a Mathematica application to generate numerical codes for tensorial evolution equations,” *Comput. Phys. Commun.* **174**, 983–1004 (2006), arXiv:gr-qc/0404023.
- [41] Kranc, “Kranc: Kranc assembles numerical code,” .
- [42] Lars Andersson, Marc Mars, and Walter Simon, “Local existence of dynamical and trapping horizons,” *Phys. Rev. Lett.* **95**, 111102 (2005), arXiv:gr-qc/0506013 [gr-qc].
- [43] Lars Andersson, Marc Mars, and Walter Simon, “Stability of marginally outer trapped surfaces and existence of marginally outer trapped tubes,” *Adv. Theor. Math. Phys.* **12** (2008), arXiv:0704.2889 [gr-qc].
- [44] Lars Andersson, Marc Mars, Jan Metzger, and Walter Simon, “The Time evolution of marginally trapped surfaces,” *Class. Quant. Grav.* **26**, 085018 (2009), arXiv:0811.4721 [gr-qc].
- [45] Ivan Booth and Stephen Fairhurst, “Isolated, slowly evolving, and dynamical trapping horizons: geometry and mechanics from surface deformations,” *Phys. Rev. D* **75**, 084019 (2007), arXiv:gr-qc/0610032.
- [46] Changjun Gao, Xuelei Chen, Valerio Faraoni, and You-Gen Shen, “Does the mass of a black hole decrease due to the accretion of phantom energy,” *Phys. Rev. D* **78**, 024008 (2008), arXiv:0802.1298 [gr-qc].
- [47] José Luis Jaramillo, “A Young-Laplace law for black hole horizons,” *Phys. Rev. D* **89**, 021502 (2014), arXiv:1309.6593 [gr-qc].
- [48] José Luis Jaramillo, “Black hole horizons and quantum charged particles,” *Class. Quant. Grav.* **32**, 132001 (2015), arXiv:1410.0509 [gr-qc].
- [49] Jos Luis Jaramillo, “A perspective on Black Hole Horizons from the Quantum Charged Particle,” *Proceedings, Spanish Relativity Meeting: Almost 100 years after Einstein Revolution (ERE 2014): Valencia, Spain, September 1-5, 2014*, *J. Phys. Conf. Ser.* **600**, 012037 (2015), arXiv:1608.05963 [gr-qc].
- [50] P.C. Vaidya, “The External Field of a Radiating Star in Relativity,” *Gen. Rel. Grav.* **31**, 119–120 (1999).
- [51] J.R. Oppenheimer and H. Snyder, “On Continued gravitational contraction,” *Phys. Rev.* **56**, 455–459 (1939).
- [52] Ivan Booth, Lionel Brits, Jose A. Gonzalez, and Chris Van Den Broeck, “Marginally trapped tubes and dynamical horizons,” *Class. Quant. Grav.* **23**, 413–440 (2006), arXiv:gr-qc/0506119 [gr-qc].
- [53] Alexis Helou, Ilia Musco, and John C. Miller, “Causal Nature and Dynamics of Trapping Horizons in Black Hole Collapse,” *Class. Quant. Grav.* **34**, 135012 (2017), arXiv:1601.05109 [gr-qc].
- [54] Ayan Chatterjee, Amit Ghosh, and Suresh Jaryal, “Marginally Trapped Surfaces in Spherical Gravitational Collapse,” (2020), arXiv:2004.11266 [gr-qc].
- [55] Ivan Booth, “Spacetime near isolated and dynamical trapping horizons,” *Phys. Rev. D* **87**, 024008 (2013), arXiv:1207.6955 [gr-qc].
- [56] Erik Schnetter, Badri Krishnan, and Florian Beyer, “Introduction to dynamical horizons in numerical relativity,” *Phys. Rev. D* **74**, 024028 (2006), arXiv:gr-qc/0604015.
- [57] Anshu Gupta, Badri Krishnan, Alex Nielsen, and Erik Schnetter, “Dynamics of marginally trapped surfaces in a binary black hole merger: Growth and approach to equilibrium,” *Phys. Rev. D* **97**, 084028 (2018), arXiv:1801.07048 [gr-qc].
- [58] Abhay Ashtekar and Gregory J. Galloway, “Some uniqueness results for dynamical horizons,” *Adv. Theor. Math. Phys.* **9**, 1–30 (2005), arXiv:gr-qc/0503109.
- [59] Raphael Bousso and Netta Engelhardt, “Proof of a New Area Law in General Relativity,” *Phys. Rev. D* **92**, 044031 (2015), arXiv:1504.07660 [gr-qc].
- [60] Raphael Bousso and Netta Engelhardt, “New Area Law in General Relativity,” *Phys. Rev. Lett.* **115**, 081301 (2015), arXiv:1504.07627 [hep-th].
- [61] Fabio Sanches and Sean J. Weinberg, “Refinement of the Bousso-Engelhardt Area Law,” *Phys. Rev. D* **94**, 021502 (2016), arXiv:1604.04919 [hep-th].
- [62] Abhay Ashtekar, Stephen Fairhurst, and Badri Krishnan, “Isolated horizons: Hamiltonian evolution and the first law,” *Phys. Rev. D* **62**, 104025 (2000), arXiv:gr-qc/0005083.
- [63] Badri Krishnan, “The spacetime in the neighborhood of a general isolated black hole,” *Class. Quant. Grav.* **29**, 205006 (2012), arXiv:1204.4345 [gr-qc].
- [64] Abhay Ashtekar, Christopher Beetle, and Jerzy Lewandowski, “Mechanics of Rotating Isolated Horizons,” *Phys. Rev. D* **64**, 044016 (2001), arXiv:gr-qc/0103026.
- [65] Abhay Ashtekar, Christopher Beetle, and Jerzy Lewandowski, “Geometry of Generic Isolated Horizons,” *Class. Quant. Grav.* **19**, 1195–1225 (2002), arXiv:gr-qc/0111067.
- [66] Jerzy Lewandowski, “Spacetimes Admitting Isolated Horizons,” *Class. Quant. Grav.* **17**, L53–L59 (2000), arXiv:gr-qc/9907058.
- [67] Sharmila Gunasekaran and Ivan Booth, “Horizons as boundary conditions in spherical symmetry,” *Phys. Rev. D* **100**, 064019 (2019), arXiv:1905.02748 [gr-qc].
- [68] Norman Gürlebeck, “No-hair theorem for Black Holes in Astrophysical Environments,” *Phys. Rev. Lett.* **114**, 151102 (2015), arXiv:1503.03240 [gr-qc].
- [69] Ales Flandera, “Geometry of isolated horizons,” (2016), arXiv:1611.02215 [gr-qc].
- [70] Jerzy Lewandowski and Tomasz Pawłowski, “Neighborhoods of isolated horizons and their stationarity,” *Class. Quant. Grav.* **31**, 175012 (2014), arXiv:1404.7836 [gr-qc].
- [71] Jerzy Lewandowski and Carmen Li, “Spacetime near Kerr isolated horizon,” (2018), arXiv:1809.04715 [gr-qc].
- [72] Martin Scholtz, Ales Flandera, and Norman Gürlebeck, “Kerr-Newman black hole in the formalism of isolated horizons,” *Phys. Rev. D* **96**, 064024 (2017), arXiv:1708.06383 [gr-qc].
- [73] Robert P. Geroch and J. B. Hartle, “Distorted black holes,” *J. Math. Phys.* **23**, 680 (1982).
- [74] Stephen Fairhurst and Badri Krishnan, “Distorted black holes with charge,” *Int. J. Mod. Phys. D* **10**, 691–710 (2001), arXiv:gr-qc/0010088.
- [75] Terry Pilkington, Alexandre Melanson, Joseph Fitzgerald, and Ivan Booth, “Trapped and marginally trapped surfaces in Weyl-distorted Schwarzschild solutions,” *Class. Quant. Grav.* **28**, 125018 (2011), arXiv:1102.0999 [gr-qc].
- [76] Abhay Ashtekar and Badri Krishnan, “Dynamical horizons: Energy, angular momentum, fluxes and balance laws,” *Phys. Rev. Lett.* **89**, 261101 (2002), arXiv:gr-

- qc/0207080.
- [77] Abhay Ashtekar and Badri Krishnan, “Dynamical horizons and their properties,” *Phys. Rev.* **D68**, 104030 (2003), arXiv:gr-qc/0308033.
 - [78] S.A. Hayward, “General laws of black hole dynamics,” *Phys.Rev.* **D49**, 6467–6474 (1994).
 - [79] Sean A. Hayward, “Spin coefficient form of the new laws of black hole dynamics,” *Class. Quant. Grav.* **11**, 3025–3036 (1994), arXiv:gr-qc/9406033.
 - [80] Sean A. Hayward, “Energy and entropy conservation for dynamical black holes,” *Phys. Rev.* **D70**, 104027 (2004), arXiv:gr-qc/0408008.
 - [81] Sean A. Hayward, “Angular momentum conservation for dynamical black holes,” *Phys. Rev.* **D74**, 104013 (2006), arXiv:gr-qc/0609008.
 - [82] Ivan Booth and Stephen Fairhurst, “The first law for slowly evolving horizons,” *Phys. Rev. Lett.* **92**, 011102 (2004), arXiv:gr-qc/0307087.
 - [83] Vaishak Prasad, Anshu Gupta, Sukanta Bose, Badri Krishnan, and Erik Schnetter, “News from horizons in binary black hole mergers,” (2020), arXiv:2003.06215 [gr-qc].
 - [84] T. Damour, *Quelques propriétés mécaniques, électromagnétiques, thermodynamiques et quantiques des trous noirs*, Ph.D. thesis, University of Paris (1979).
 - [85] Thibaut Damour, *Surface effects in black hole physics* (na, 1982).
 - [86] R. H. Price and K. S. Thorne, “Membrane Viewpoint on Black Holes: Properties and Evolution of the Stretched Horizon,” *Phys. Rev.* **D33**, 915–941 (1986).
 - [87] K. S. Thorne, R. H. Price, and D. A. MacDonald, *Black holes: The membrane paradigm* (Yale University Press, 1986).
 - [88] Eric Gourgoulhon, “A generalized Damour-Navier-Stokes equation applied to trapping horizons,” *Phys. Rev.* **D72**, 104007 (2005), arXiv:gr-qc/0508003.
 - [89] Eric Gourgoulhon and Jose Luis Jaramillo, “Area evolution, bulk viscosity and entropy principles for dynamical horizons,” *Phys. Rev.* **D74**, 087502 (2006), arXiv:gr-qc/0607050.
 - [90] Eric Gourgoulhon and Jose Luis Jaramillo, “New theoretical approaches to black holes,” *New Astron. Rev.* **51**, 791–798 (2008), arXiv:0803.2944 [astro-ph].
 - [91] Abhay Ashtekar, Christopher Beetle, and Stephen Fairhurst, “Isolated horizons: A generalization of black hole mechanics,” *Class. Quant. Grav.* **16**, L1–L7 (1999), arXiv:gr-qc/9812065.
 - [92] Abhay Ashtekar, Christopher Beetle, and Stephen Fairhurst, “Mechanics of Isolated Horizons,” *Class. Quant. Grav.* **17**, 253–298 (2000), arXiv:gr-qc/9907068.
 - [93] Abhay Ashtekar and Alejandro Corichi, “Laws governing isolated horizons: Inclusion of dilaton couplings,” *Class. Quant. Grav.* **17**, 1317–1332 (2000), arXiv:gr-qc/9910068.
 - [94] Jacob D. Bekenstein, “Black holes and entropy,” *Phys. Rev.* **D7**, 2333–2346 (1973).
 - [95] James M. Bardeen, B. Carter, and S. W. Hawking, “The Four laws of black hole mechanics,” *Commun. Math. Phys.* **31**, 161–170 (1973).
 - [96] Sayantani Bhattacharyya, Veronika E Hubeny, Shiraz Minwalla, and Mukund Rangamani, “Nonlinear Fluid Dynamics from Gravity,” *JHEP* **02**, 045 (2008), arXiv:0712.2456 [hep-th].
 - [97] Ivan Booth, Michal P. Heller, Grzegorz Plewa, and Michal Spalinski, “On the apparent horizon in fluid-gravity duality,” *Phys. Rev. D* **83**, 106005 (2011), arXiv:1102.2885 [hep-th].
 - [98] Pau Figueras, Veronika E. Hubeny, Mukund Rangamani, and Simon F. Ross, “Dynamical black holes and expanding plasmas,” *JHEP* **04**, 137 (2009), arXiv:0902.4696 [hep-th].
 - [99] Li-Ming Cao, “Deformation of Codimension-2 Surface and Horizon Thermodynamics,” *JHEP* **03**, 112 (2011), arXiv:1009.4540 [gr-qc].
 - [100] Jose Luis Jaramillo, Rodrigo P. Macedo, Philipp Mösta, and Luciano Rezzolla, “Black-hole horizons as probes of black-hole dynamics II: geometrical insights,” *Phys. Rev.* **D85**, 084031 (2012), arXiv:1108.0061 [gr-qc].
 - [101] J. L. Jaramillo, R. P. Macedo, P. Mösta, and L. Rezzolla, “Towards a cross-correlation approach to strong-field dynamics in Black Hole spacetimes,” *Proceedings, Spanish Relativity Meeting : Towards new paradigms. (ERE 2011): Madrid, Spain, August 29-September 2, 2011*, AIP Conf. Proc. **1458**, 158–173 (2011), arXiv:1205.3902 [gr-qc].
 - [102] Richard H. Price, Gaurav Khanna, and Scott A. Hughes, “Systematics of black hole binary inspiral kicks and the slowness approximation,” *Phys.Rev.* **D83**, 124002 (2011), arXiv:1104.0387 [gr-qc].
 - [103] Gregory J. Galloway, “Maximum principles for null hypersurfaces and null splitting theorems,” *Annales Henri Poincaré* **1**, 543–567 (2000), arXiv:math/9909158.
 - [104] Aron C. Wall, “The Generalized Second Law implies a Quantum Singularity Theorem,” *Class. Quant. Grav.* **30**, 165003 (2013), [Erratum: *Class.Quant.Grav.* **30**, 199501 (2013)], arXiv:1010.5513 [gr-qc].
 - [105] T. Padmanabhan, “Entropy density of spacetime and the navier-stokes fluid dynamics of null surfaces,” *Phys. Rev. D* **83**, 044048 (2011).
 - [106] Ricardo Uribe-Vargas, “On singularities, perestroikas and differential geometry of space curves,” *L’Enseignement Mathématique. IIe Série* **50** (2004), 10.5169/seals-2641.
 - [107] V.I. Arnold and International Mathematical Union, *Contact Geometry and Wave Propagation: Lectures Given at the University of Oxford Under the Sponsorship of the International Mathematical Union*, Monographie de l’Enseignement mathématique (L’Enseignement mathématique, Université de Genève, 1989).
 - [108] H. Friedrich and J.M. Stewart, “Characteristic initial data and wave front singularities in general relativity,” *Proc. Roy. Soc. Lond. A* **A385**, 345–371 (1983).
 - [109] Jürgen Ehlers and Ezra Newman, “The theory of caustics and wave front singularities with physical applications,” *Journal of Mathematical Physics*, v.41, 3344–3378 (2000) **41** (2000), 10.1063/1.533316.
 - [110] V. Arnold, *Singularities of Caustics and Wave Fronts*, Mathematics and its Applications (Springer Netherlands, 2013).